Università degli Studi di Salerno

Facoltà di Scienze Matematiche Fisiche e Naturali

Dipatimento di Chimica e Biologia

TESI DI DOTTORATO DI RICERCA IN CHIMICA

Polymorphism and co-crystalline phases of polymers

Tutor
Prof. Gaetano Guerra

PhD student
Gianluca Fasano
Matr. 8880700098

X Ciclo – Nuova serie- a.a. 2011-2012

Index

Chapter 3:   Chiral co-crystalline phases PPO/alpha pinene

Chapter 4:   Experimental section

List of Abbreviations

CCl$_4$: carbon tetrachloride

CD: circular dichroism

CE: cyclohexane

CP: cyclopentane

DCE: 1,2.dichloethane

i-P4MP1: isotactic poly(4-methyl-pentene-1)

PPO: Poly(2,6-dimethyl-1,4-phenylene)oxide

RT: room temperature

s-PS: syndiotactic polystyrene

TMB: 1,3,5-trymethylbenzene

VCD: vibrational circular dichroism

VOC: volatile organic compounds

INTRODUCTION

Crystalline phases are extremely relevant for properties and applications of many polymeric materials. In fact, their amount, structure and morphology constitute the main factors controlling physical properties of fibers, films and thermoplastics[1,2] and can be also relevant for properties of rubbers[3,4] and gels.[5,6]

It is also well known that processing and physical properties of polymer-based materials are strongly affected by the occurrence of *polymorphism* (i.e. the possibility for a given polymer to crystallize in different crystalline forms)[1,7] and *mesomorphism* (i.e. the occurrence of "disordered" crystalline phases, characterized by a degree of structural organization that is intermediate between those identifying crystalline and amorphous phases).[7,8]

Different has been the destiny of polymeric *co-crystalline forms*, i.e. structures were a polymeric host and a low-molecular-mass guest are co-crystallized.

Systems composed of solid polymers and of low molecular mass molecules find several practical applications, including advanced applications. In several cases, additives (often improperly referred as guest molecules) are simply dispersed at molecular level in polymeric amorphous phases, although frequently, to reduce their diffusivity, the active molecules are covalently attached to the polymer backbone, either by polymerization of suitable monomeric units or by grafting the active species onto preformed polymers.

A more simple alternative method to reduce diffusivity of active molecules in solid polymers and to prevent their self-aggregation consists in the formation of co-crystals with suitable polymer hosts.

Polymeric co-crystalline forms are quite common for several regular and stereoregular polymers, like e.g. isotactic and syndiotactic polystyrene (s-PS), syndiotactic poly-*p*-methyl-styrene, syndiotactic poly-*m*-methyl-styrene, syndiotactic poly-*p*-chloro-styrene, syndiotactic poly-*p*-fluoro-styrene, polyethyleneoxide, poly(muconic acid), polyoxacyclobutane, poly(vinylidene fluoride), syndiotactic polymethylmethacrylate.

The removal of the low-molecular-mass guest molecules from co-crystals can generate nanoporous-crystalline phases. In this respect, it is worth noting that nanoporous crystalline structures can be achieved for a large variety of chemical compounds: inorganic (e.g., zeolites), metal-organic as well as organic. These materials, often referred as inorganic, metal-organic and organic "frameworks" are relevant for molecular storage, recognition and separation techniques.

The removal of the low-molecular-mass guest molecules from polymer co-crystalline forms generates host chain rearrangements, generally leading to crystalline forms that, as usual for polymers, exhibit a density higher than that one of the corresponding amorphous phase. However,

in few cases (to our knowledge, up to now only for s-PS), by using suitable guest removal conditions,[9] nanoporous crystalline forms, exhibiting a density definitely lower than that of the corresponding amorphous phases are obtained.

s-PS has been widely studied and characterized in recent years. This polymer has a complex and widely studied polymorphism, it has 5 crystal structures, α, β, γ, δ, ε, and a wide variety of co-crystal structures with different low molecular weight molecules. [10]

The removal of the low-molecular-mass guest molecules from s-PS co-crystals can generate two different nanoporous-crystalline phases.

The first polymeric nanoporous-crystalline form, the δ form of s-PS, was discovered and patented in 1994.[11] The crystal structure of the δ form has been determined by the analysis of X-ray fiber diffraction patterns and packing energy calculations. Chains in the helical s(2/1)2 conformation are packed in a monoclinic unit cell with axes $a = 1.74$ nm, $b = 1.185$ nm, $c = 0.77$ nm, and $\gamma = 117°$, according to the space group $P2_1/a$ (Figure 1, upper part).[12] The calculated density is of 0.98 g cm^{-3}, i.e. definitely smaller than that one of the amorphous phase (1.05 g cm^{-3}).

The nanoporous ε phase of s-PS, discovered only in 2007 [13], presents an orthorhombic unit cell with axes $a = 1.61$ nm, $b = 2.18$ nm and $c = 0.79$ nm (Figure 1, lower part).[14] Four chains of s-PS in the s(2/1)2 helical conformation are included in the unit cell, whose calculated density is 0.98 g cm^{-3}, i.e. very close to the density established for the δ phase.
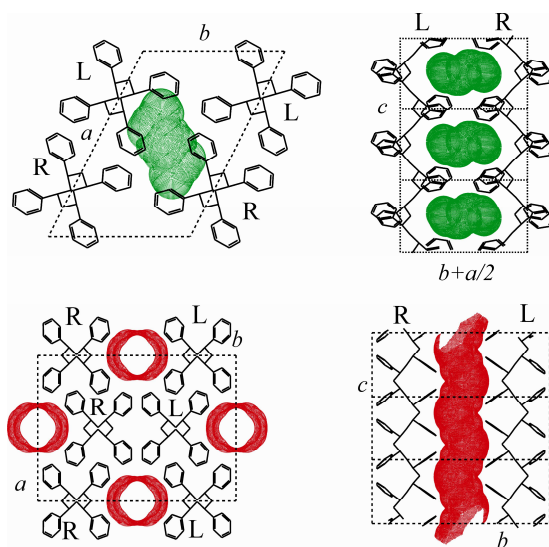

Figure 1. *Top and lateral views of the crystalline structures of the two nanoporous crystalline forms of s-PS. For the δ (upper Figures) and ε (lower Figures) forms, the porosity is distributed as cavities and channels, respectively.*

Several sorption studies have shown that the δ and ε nanoporous crystalline phases are able to sorb volatile organic compounds (both from gas phase and aqueous solutions from water and air), also when present at very low concentrations[15]. This makes these new materials particularly interesting for potential industrial applications in water or air purification.

A relevant feature of the s-PS nanoporous crystalline phases is the possibility to be obtained with different kinds of uniplanar orientations, by using suitable processes of film production. The degree and the kind of uniplanar orientation depends on the selected technique (solution crystallization procedures or solvent induced crystallization in amorphous samples or solvent induced re-crystallizations of γ and α unoriented samples

Several studies have shown the possibility to form δ related and ε related co-crystalline phases with non-linear optical, fluorescent, polar, paramagnetic, photoreactive and chiral guest molecules.[17] The possibility to achieve s-PS film with three different kinds of uniplanar orientation allows controlling the orientation of the guest molecules not only in the microscopic crystalline phase but also in macroscopic films.

On these bases, films presenting s-PS/active-guest co-crystalline phases have been proposed as advanced materials, mainly as optical (chromophore, fluorescent, photo-reactive), ferroelectric and paramagnetic materials.[18] This constitutes an innovative approach in the area of functional polymeric materials, which are instead generally characterized by a disordered distribution of active groups into amorphous phases.

Considering the knowledge and the procedures gained by studying the co-crystal structures of s-PS, this research project focused on the study of polymorphism of polymers forming co-crystalline phase with the main objective to establish the formation of nanoporous crystalline phases obtained after removal of guest molecules from the co-crystalline phases and then to carry out a detailed characterization of the obtained nanoporous forms.

In particular, two polymers have been considered in this work: isotactic poly(4-methyl-pentene-1) (i-P4MP1) and poly(2,6-dimethyl-1,4-phenylene)oxide (PPO).

Poly-4-methyl-1-pentene isotactic (i-P4MP1) is a polymer characterized by a complex polymorphism and 5 different crystalline forms, some of which are obtainable only by crystallization with solvent, [19] have been described in the literature. The study of aerogels and polymorphism of i-P4MP1 which is presented in the Chapter 1 has been the topic of a publication in *ACS Applied Materials & Interfaces:*

***Aerogels and Polymorphism of Isotactic Poly(4-methyl-pentene-1)**, Daniel C., Vitillo J. G., Fasano G., Guerra G., 2011, 3, 969.*

The second and third chapters deal with the study of poly(2,6-dimethyl-1,4-phenylene)oxide (PPO), i.e. a linear regular polymer, which as s-PS has the advantage to be a commercial thermoplastic polymer. PPO exhibits a high free volume or ultrapermeable amorphous phase and has been recognized as a membrane material with high permeation parameters.[20] Although few papers have recognized that PPO crystalline phases can play a role in gas sorption and transport processes, [20e, 21] no correlation between the amount or nature of the crystalline phase and guest sorption properties has been reported. This is mainly due to the scarce information available in the literature relative to the crystalline phases of PPO.[21,22]

In particular in the second chapter it will be shown that nanoporous crystalline phases can be obtained by removal of the solvent from PPO gels by using supercritical carbon dioxide extraction procedure. This work has been the topic of a publication in *Chemistry of Materials*:

Nanoporous Crystalline Phases of Poly(2,6-Dimethyl-1,4-phenylene)oxide, *Daniel C., Longo S., Fasano G., Vitillo J. G., Guerra G., 2011, 23, 3195.*

Finally, in the third chapter the preparation procedures, the thermal stability of the co-crystalline phase and FTIR and VCD analysis are presented. Moreover, an accurate structural analysis of the powder diffraction patterns has been carried out by Prof. V. Petraccone and Dr. O. Tarallo from the Dipartimento di Chimica "Paolo Corradini" of the Università degli Studi di Napoli Federico II. In particular co-crystalline phases with racemic and non-racemic guest molecules have been prepared and characterized. The experimental data indicates that the PPO/α-pinene co-crystalline form is chiral, i.e. the unit cell includes all right or left handed polymer helices and (1S-(–) or (1R)-(+) α-pinene guest molucules, respectively. This work is the topic of a publication in preparation:

A Chiral Co-Crystalline Form of Poly(2,6-dimethyl-1,4-phenylene)oxide (PPO),*Tarallo O., Petraccone V., Daniel C., Fasano G., Rizzo P., Guerra G.*

References

1. Tashiro K., Tadokoro, H., *In Encyclopedia of Polymer Science and Engineering. Supplement* **1989**, 187.

2. Corradini P., Auriemma F., De Rosa C., *Account of Chemical Research,* **2006**, (39), 314

3. Toki S., Fujimaki T., Okuyama M., *Polymer,* **2000**, (41), 5423.

4. Guerra G., Galimberti M., Piemontesi F., Ruiz de Ballesteros O., *Journal of American Chemical Society,* **2002**, (124), 1566.

5. Guenet J. M., *In Thermoreversible Gelation of Polymers and Biopolymers*; Academic Press: London **1992**.

6. Guenet J.M., *In Polymer-Solvent Molecular Compounds,* Elsevier Ltd.: Oxford **2008**.

7. Corradini P., Guerra G., *Advanced Polymer Science,* **1992**, (100), 183.

8. Auriemma F., De Rosa C., Corradini, P., *Advanced. Polymer Science,* **2005**, (181), 1.

9. a)Reverchon E., Guerra G., Venditto V., *Journal of Applied Polymer Science* **1999**, (74), 2077; b) Ma W., Yu J., He J., *Macromolecules* **2005**, (38), 4755.

10. a)Chatani Y., Shimane Y., Inagaki, T., Ijitsu T., Yukinari T., Shikuma H., *Polymer,* **1993**, 34, 1620, b) De Rosa C., Rizzo P., Ruiz de Ballesteros O., Petraccone V.; Guerra G., *Polymer, 19***99,** 40, 2103 c) Tarallo O., Petraccone V., *Macromolecules,* **2004,** 205, 1351.

11. Guerra G., Manfredi C., Rapacciuolo M., Corradini P., Mensitieri G., Del Nobile M. A., *Ital. Patent IT1228915,* **1994**.

12. De Rosa C., Guerra G., Petraccone V., Pirozzi B., *Macromolecules* **1997**, (30), 4147.

13. Rizzo P., Daniel C., De Girolamo Del Mauro A., Guerra G., *Chemistry of Materials,* **2007**, (19), 3864.

14. Petraccone V., Ruiz de Ballesteros, O., Tarallo O., Rizzo P., Guerra G., *Chemistry of Materials,* **2008**, (20), 3663.

15. Guerra G., Manfredi C., Musto P., Tavone S., *Macromolecules,* **1998**, (31), 1329.

16. Albunia A.R., Rizzo P., Guerra G., *Chemistry of Materials,* **2009**, (21), 3370.

17. a) Uda Y., Kaneko F., Tanigaki N., Kawaguchi T., *Advanced Materials* **2005** (17), 1846; b) De Girolamo Del Mauro A., Carotenuto M., Venditto V., Petraccone V., Scoponi M., Guerra G., *Chemistry of Materials,* **2007**, (19), 6041**.**

18. Giordano M., Russo M., Cusano A., Mensitieri G., Guerra, G., *Sensors and Actuators B,* **2005**, (109), 177.

19. De Rosa C., Borriello A., Venditto V., Corradini P., *Macromolecules,* **1994**, (27), 3864.

20. a) Yasuda H., Rosengren K., *Journal of Applied Polymer Science,* **1970**, (14), 2839; b) Chern R.Y., Sheu F.R., Jia L., Stannet V.T., Hopfenbewrg H.B., *Journal of Membrane*

Science, **1987**, (35), 103; c) Ilinitch O.M., Semin G.L., Chertova M.V., Zamaraev K.I., *Journal of Membrane Science* **1992**, (66), 1; d) Aguilar-Vega M., Paul D. R., *Journal of Polymer Science. Part B: Polym. Phys.,* **1993**, (31), 1577; e) Ilinitch O.M., Fenelov V.B., Lapkin A.A., Okkel L.G., Terskikh V.V., Zamaraev K.I., *Microporous Mesoporous Materials.* **1999**, (31), 97; f) Khayet M., Villaluenga J.P.G., Godino M.P., Mengual J.I., Seoane B., Khulbe K.C., Matsuura T., *Journal of Colloid and Interface Science* **2004**, (278), 410; g) Pourafshari Chenar M., Soltanieh M., Matsuura T., Tabe-Mohammadi A., Khulbe K.C., *Journal of Membrane Science* **2006**, (285), 265; h) Sterescu D.M., Stamatialis D.F., Mendes E., Kruse J., Rätzke K., Faupel F., Wessling M., *Macromolecules* **2007**, (40)**,** 5400.

21. a) Alentiev A., Drioli E., Gokzhaev M., Golemme G., Ilinich O.M., Lapkin A.A., Volkov V., Yampolskii Yu., *Journal of Membrane Science,* **1998**, (138), 99; b) Khulbe K.C., Matsuura T., Lamarche G., Lamarche A.-M., *Journal of Membrane Science,* **2000**, (170), 81.

22. a) Packter A., Sharif K.A., *Journal of Polymer Science, Polym.Lett.Ed.,* **1971**, (9)*,* 435; b) Guerra G., De Rosa C., Vitagliano V.M., Petraccone V., Corradini P., *Journal of Polymer Science, partB:Polymer Physics,* **1991**, (29)*,* 265; c) Sterescu D.M., Stamatialis D.F., Mendes E., Wübbenhorst M., Wessling M., *Macromolecules,* **2006**, **(**39)**,** 9234.

Chapter 1

Polymorphism and aerogels of Isotactic Poly(4-methyl-pentene-1)

1.1 Introduction

Isotactic poly(4-methyl-pentene-1) (i-P4MP1) is a semi-crystalline polymer with different properties (high melting point, high clarity, good electrical properties and chemical resistance) being suitable for many applications such as coating of electrical wires, food packaging or optical components.[1] Moreover i-P4MP1 is one of the most permeable plastics to gases and thus is of practical importance as a membrane making polymer.[2-3]

$$-[CH_2-CH]-$$
$$|$$
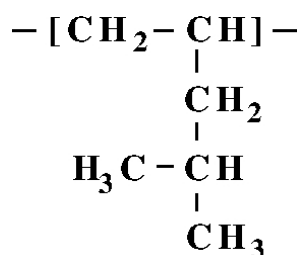$$CH_2$$
$$|$$
$$H_3C-CH$$
$$|$$
$$CH_3$$

Figure 1.1 Chemical structure of i-P4MP1 repeating unit

I-P4MP1 presents a complex polymorphic behavior, which is made more complicated by different nomenclatures existing in the literature. Depending on the crystallization procedures, at least four different crystalline forms have been reported. Form I, which is the most stable crystalline form, can be obtained from the melt or from crystallization in high boiling solvents.[4-7] Form I is characterized by polymer chains assuming a 7_2 helical conformation (see Figure 1) and a chain packing in a tetragonal unit cell with $a = 18.66$ Å and $c = 13.80$ Å.[4-6] Form II, which can be obtained by isothermal crystallization from dilute xylene solutions at 25°C, is characterized by a 4_1 helical chain conformation[8-10] and a chain packing in a monoclinic unit cell[9,10] with $a = 10.49$ Å, $b = 18.89$ Å and $c = 7.13$ Å and $\gamma = 113.7°$.[9] A 4_1 helical chain conformation is also present in Form III, which is typically obtained by crystallization from dilute solutions in xylene at 65°C[8], in decalin,[11-13] in linear and branched alkanes,[7] as well as in carbon tetrachloride and cycloalkanes.[6] Form III is characterized by a tetragonal unit cell ($a = 19.46$ Å, $c = 7.02$ Å).[12,13] Form IV can be obtained by annealing of form I at high temperature (above 200°C) under pressure (above 4500

atm)[14] or by crystallization from cyclopentane solutions.[14-16] This crystalline form is characterized by a hexagonal unit cell (a = 22.17 Å, c = 6.5 Å) and a 3_1 chain conformation.[15,16]

As many other polymers, i-P4MP1 can form thermoreversible gels in a large variety of solvents.[15, 17-20] Depending on the solvent, the physical cross-links of i-P4MP1 gels can present different crystalline forms.[15,17] For instance, diffraction patterns typical of Form I and form IV were obtained after drying of gel with decalin[17] and cyclopentane,[15.] respectively. Moreover depending on the gelation conditions, different crystalline structures can be obtained with a same solvent.[19]

It is also worth noting that an additional crystalline structure which have been provisionally indicated as forms V have been obtained in cyclohexane gels[17] and by crystallization in cyclohexane and carbon tetrachloride solutions.[21]

7/2 helix
FORM I
ρ_c=0.822 g/cm³

4/1 helix
FORM II   FORM III
ρ_c=0.862 g/cm³ ρ_c=0.851 g/cm³

3/1 helix
FORM IV
ρ_c=0.907 g/cm³

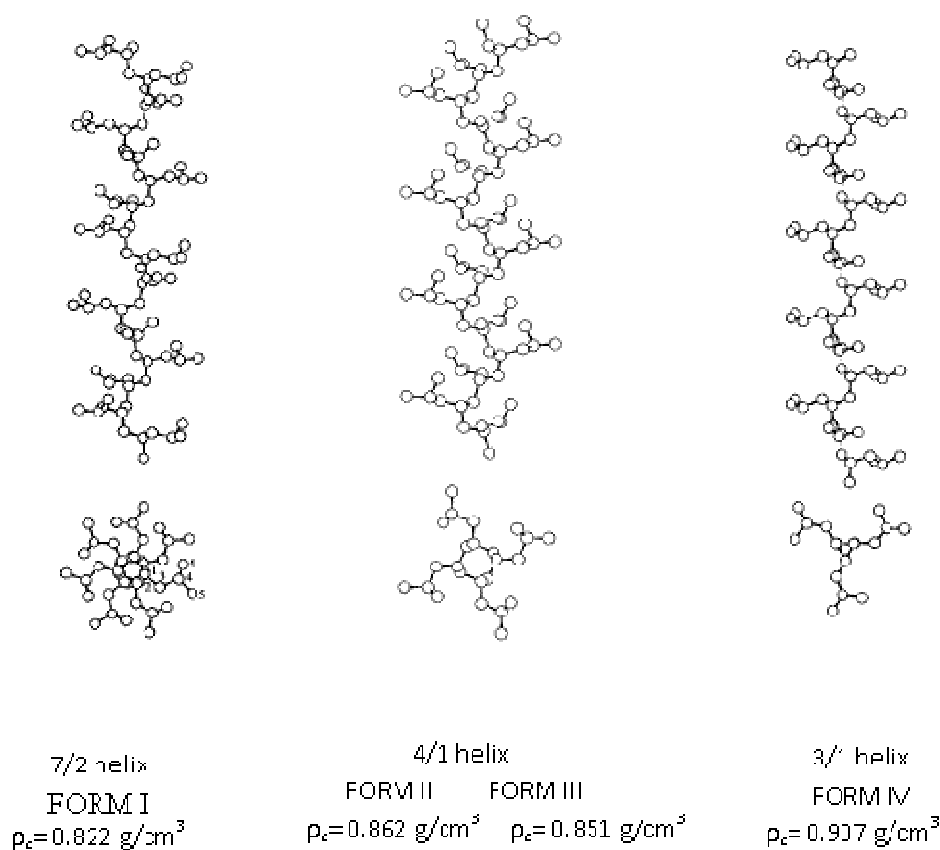***Figure 1.2*** *Side view and projection along the chain axis of the chain conformation in the crystalline phases of i-P4MP1. The density of the different crystalline forms is also reported.*

The present chapter reports on the preparation of i-P4MP1 aerogels, starting from gels obtained with several different solvents with the aim to establish the possible formation of nanoporous crystalline phases after solvent removal from the gels.

The first part will be focussed on the X-ray diffraction investigations of the polymorphism of i-P4MP1 gels prepared with different solvents and of corresponding desiccated gels in order to establish the possible formation of co-crystalline phases. In the second part, highly porous aerogels obtained from the different gels will be prepared by extraction with supercritical carbon dioxide and results concerning their crystalline structure, morphology and porosity will be presented and discussed.

1.2 I-P4MP1 gels

1.2.1 Gels with pure polymer crystalline phases

Different gels have been prepared in 1,3,5-trimethylbenzene (TMB), decalin and cyclopentane (CP).

In Figure 1.3 are reported the X-ray diffraction patterns of i-P4MP1 gels prepared in TMB (Figure 1.3A), decalin (Figure 1.3B) and CP (Figure 1.3C) during the progressive desorption of solvent at room temperature in air.
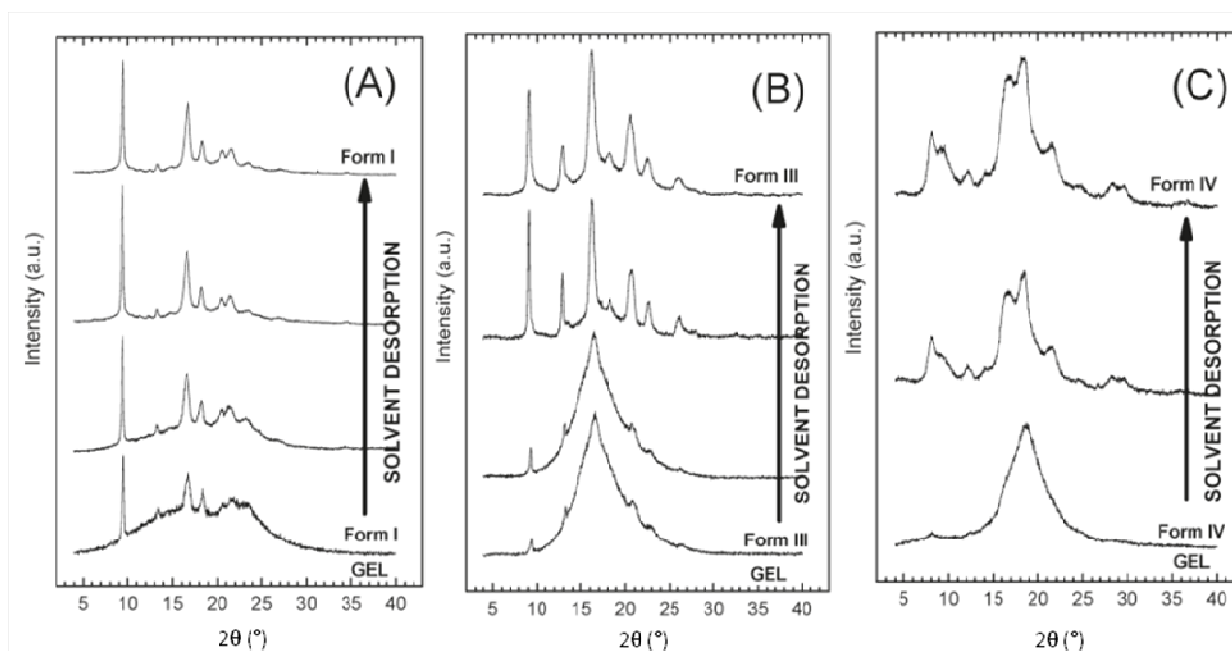
Figure 1.3 *X-ray diffraction patterns of i-P4MP1 gels prepared in 1,3,5-trimethylbenzene (A) , decalin (B) and cyclopentane (C), during the progressive desorption of solvent in air.*

It can observe in Figure 1.3 that the structure of the crystalline junctions formed in i-P4MP1 gels depends on the solvent. Forms I, III and IV are obtained in native gels prepared with TMB, decalin and cyclopentane, respectively. Then, during progressive solvent desorption the crystalline

structures do not undergo any transition and the crystalline forms of the fully dried gels are those initially present in the native gel.

The Bragg angles, the relative intensities and the indices *hkl* of the reflections observed for the totally desiccated gels are listed in table 1.1.

Table 1.1 *Diffraction angles ($2\theta_{CuK\alpha}$) and relative intensities of the reflections observed in the X-ray diffraction profiles of desiccated gels of Figure 1.2 and of the aerogel from gel with CE (Figure 1.5)*

desiccated gel with TMB (Fig. 1.3A) *Form I*			aerogel from gel with CE (Fig. 1.6) *Form II*			desiccated gel with decalin (Fig. 1.3B) *Form III*			desiccated gel with CP (Fig. 1.3C) *Form IV*		
2θ (deg)	I	(hkl)[a]	2θ (deg)	I	(hkl)[b]	2θ (deg)	I	(hkl)[c]	2θ (deg)	I	(hkl)[d]
9.45	vs	200	9.20	vs	100	9.10	vs	200	8.05	S	110
11.50	vw	201	10.30	vs	020	12.90	mw	220, 101	9.40	S	200
12.45	vw	211	10.85	m	$1\bar{2}0$	16.20	vs	211	12.10	mw	210
13.40	w	220	13.20	mw	011	18.30	vw	400,301	16.40	S	310
15.00	w	112,221	14.85	m	$1\bar{1}1$	20.65	mw	420,321	18.20	S	211
16.75	s	212	16.30	ms	021,$1\bar{2}1$	22.70	vw	411	21.15	W	311
20.70	mw	113,411	17.20	w	111,$2\bar{2}0$	26.20	vw	431,112,501	24.50	vw	401
21.65	mw	322,203	18.25	mw	200	32.60	vw	541,710,422	26.85	vw	411
23.50	w		19.70	mw	031	35.00	vw	512,701	28.35	vw	511
25.00	vw	422	20.30	mw	040,121				29.50	vw	202,212
27.00	vw	440	21.20	mw	$2\bar{2}1$				36.40	vw	531,701
34.50	vw		22.70	w	$2\bar{3}1,1\bar{4}1$						
			24.00	vw	041						
			25.80	mw	140						
			29.05	vw	141						

[a] Key: vs = very strong, ms = medium strong, s = strong, mw = medium weak, w = weak, vw = very weak
[b] hkl indices of Form I reflections taken from ref 6
[c] hkl indices of Form II reflections taken from ref 9
[d] hkl indices of Form III reflections taken from ref 12
[e] hkl indices of Form IV reflections taken from ref 16

1.2.2 *Gels with polymer-solvent co-crystalline phases*

In Figure 1.4, are reported X-ray diffraction patterns of a i-P4MP1/cyclohexane (CH) and i-P4MP1/carbon tetrachloride gels during the progressive solvent desorption.

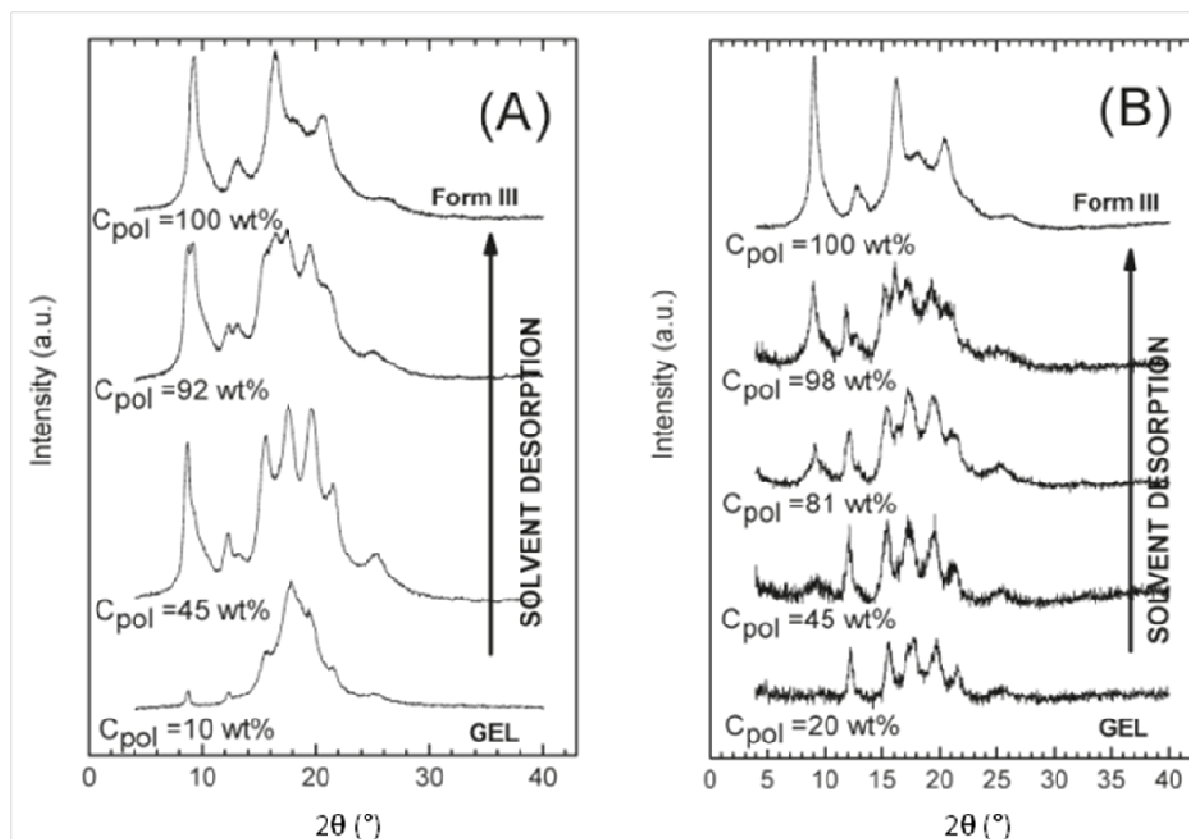***Figure 1.4.** X-ray diffraction patterns of gels prepared in cyclohexane (A) and carbon tetrachloride (B) during progressive solvent desorption in air*

The diffraction pattern of the i-P4MP1 native gels with cyclohexane and carbon tetrachloride display the diffraction peaks listed in Table 1.2, which become stronger after partial evaporation of the solvent ($C_{pol} \approx 45$ wt%).When solvent evaporation proceeds ($C_{pol} > 90\%$), new diffraction peak which can be attributed to form III become visible at $2\theta= 9.2, 13.10,$ and $16.4°$.

Finally after complete solvent evaporation (upper curves), only the diffraction peaks typical of form III (see table 1.1) are present while all the diffraction peaks initially observed in the native gel have disappeared.

The progressive substitution of the diffraction peaks of both native gels with the peaks of Form III, during the progressive solvent desorption, suggests that the native crystalline phases are polymer-solvent co-crystalline phases. This hypothesis is supported by the fact that the positions of the diffraction peaks observed in cyclohexane and CCl₄ gels are slightly different (see Table 1.2).

To further support the hypothesis of formation of two different co-crystalline phases, it is worth noting that the transition into form III is fully reversible, as exposition of form III desiccated gels to

11

cyclohexane or CCl$_4$ vapors leads again to the co-crystalline phases, exhibiting the diffraction peaks listed in Table 1.2.

Table 1.2 *Diffraction angles ($2\theta_{CuK\alpha}$) and relative intensities of the reflections observed in the X-ray diffraction profile of native gels obtained with cyclohexane and carbon tetrachloride (Figure 1.5A and B)*

Co-crystal with cyclohexane		Co-crystal with CCl$_4$	
2θ (deg)	I	2θ (deg)	I
8.7	vs		
12.3	s	12.2	s
13.3	w		
15.5	vs	15.55	s
17.6	vs	17.45	s
19.6	vs	19.7	s
21.4	w	21.55	s
25.25	w	25.5	w

Key: vs = very strong, ms = medium strong, s = strong, mw = medium weak, w = weak, vw = very weak

In this respect, it is worth noting that the crystalline structure of cross-link junctions of cyclohexane and carbontetrachloride gels have been indicated in literature as form V of i-P4MP1.

1.3 I-P4MP1 aerogels

Independently of the crystalline structure of the junction zones of the i-P4MP1 gels, complete removal of the solvent was achieved by supercritical CO$_2$ extraction procedures. The advantage of supercritical CO$_2$ drying is the absence of surface tension. During the extraction process, a supercritical solution is formed between supercritical CO$_2$ and liquid solvent and is, thus, possible to extract the solvent without collapsing the structure.

As an example, Figure 1.5 shows that the dimensions of a i-P4MP1 gel prepared in TMB at a polymer concentration C$_{pol}$ = 0.20 g/g remain substantially unchanged during the extraction and a monolithic aerogel with a total porosity of 6.2 cm^3/g and a percentage of porosity of 80% is obtained.
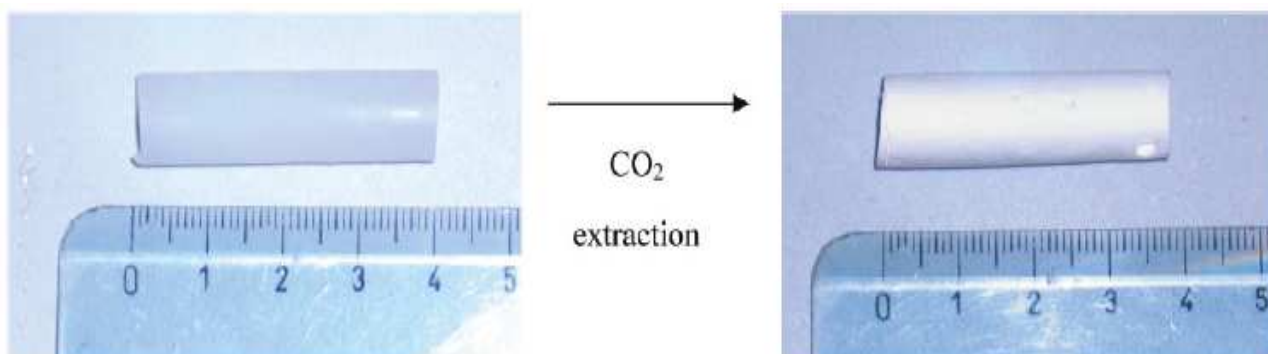
Figure 1.5 *Photographs of a piece of i-P4M1P gel prepared in TMB at C_{pol} = 0.20 g/g, before and after complete solvent extraction via supercritical carbon dioxide*

1.3.1 X-ray diffraction analysis

The complete extraction of the solvent present in native gels prepared in TMB (starting crystalline form: form I), decaline (starting crystalline form: form III), cyclopentane (starting crystalline form: form IV) and cyclohexane (starting crystalline form: co-crystal form) has been achieved with supercritical CO_2 at 40°C and 200 bar for 240 min and X-ray diffraction patterns of the samples after extraction, are reported in Figure 1.6.
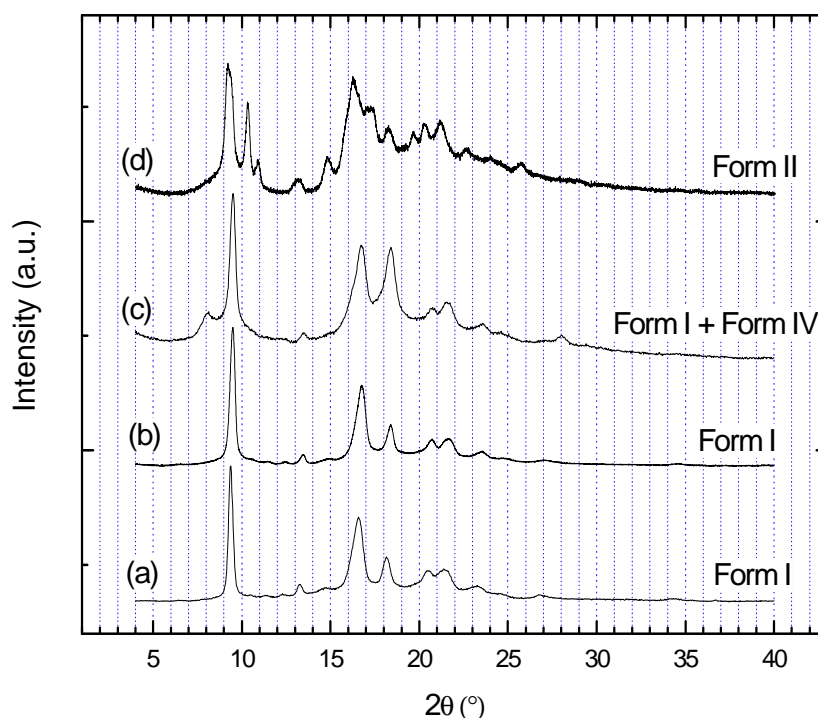

Figure 1.6 *X-ray diffraction patterns of the samples obtained from i-P4MP1 gels prepared in TMB, decaline, CP and cyclohexane after complete solvent extraction with supercritical CO_2*

We can observe, that unlike progressive solvent desorption (Figure 1.3), the abrupt extraction with carbon dioxide in supercritical conditions of solvent from gels characterized by pure polymer

13

crystalline phases leads to form I aerogels, independently of the crystalline structure of the native gel (with the exception of Form IV gel which maintains a small amount of Form IV crystallites during solvent extraction with supercritical CO_2). It is also possible to observe that both the degree crystallinity and the crystalline domains correlation length of the aerogels is particularly high. Thus, for instance, for the Form I aerogel obtained from the gel prepared in TMB (curve a of Figure 1.8) a crystallinity of c.a. 50% and a correlation length of the crystals perpendicular to the 200 plane (D_{200}) as evaluated on the basis of the half-height width of the 020 peak (at $2\theta_{CuK\alpha}$ =9.45°) of nearly 31 nm is obtained. Smaller D_{200} values are obtained with the Form I aerogels obtained from decaline (D_{200} = 26 nm) and CP (D_{200} =24 nm). This could be due to the crystalline transition occuring during solvent extraction.

Unlike i-P4MP1 gels with a pure crystalline phase, the rapid gel extraction procedure based on carbon dioxide in supercritical conditions, when applied to the gels exhibiting co-crystalline phases (with cyclohexane or CCl_4) leads to highly crystalline Form II aerogels.

This is shown for instance in curve d of Figure 1.6, where the X-ray diffraction pattern of the sample obtained from a i-P4MP1/cyclohexane gel after solvent extraction by CO_2 at 40°C and 200 bar, is reported. The diffraction pattern of the aerogel (crystallinity of c.a. 40%) displays well-resolved narrow diffraction peaks indicating the formation of large Form II crystals (see Table 1.1). For instance, the correlation length of the crystals perpendicular to the 020 plane, as evaluated on the basis of the half-height width of the 020 peak (at $2\theta_{CuK\alpha}$ =10.3°), is c.a. 32 nm.

It is worth noting that differential scanning calorimetry (DSC) analysis have shown that the II→I transition temperature for Form II aerogels occurs at 143°C which is definitely higher than those observed for form II samples obtained in different conditions (in the range 120-125°C).[8, 21]

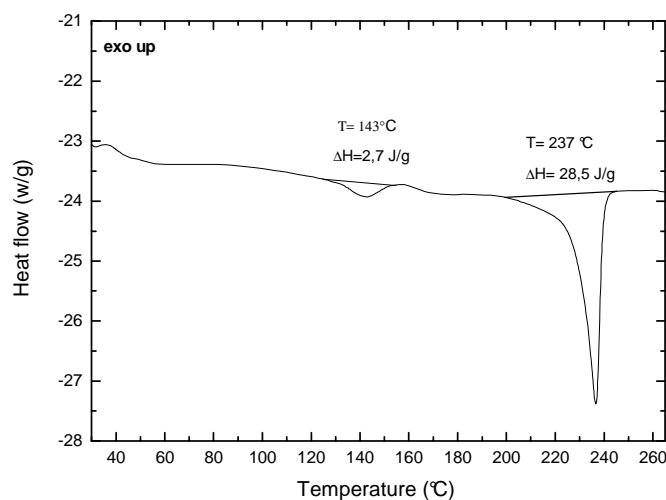

Figure 1.7 *DSC scan at 10°C/min of the Form II aerogel. It is clearly apparent a small endothermic transition ($\Delta H \approx 3$ J/g) at 143 °C beside the principal melting peak at 237°C ($\Delta H = 28.5$ J/g)*

In figure 1.8 are reported the X-ray diffraction patterns obtained after annealing at different temperatures up to 160°C. It can observe that the thermal phenomena observed just below that temperature can been attributed to the II→I transition.
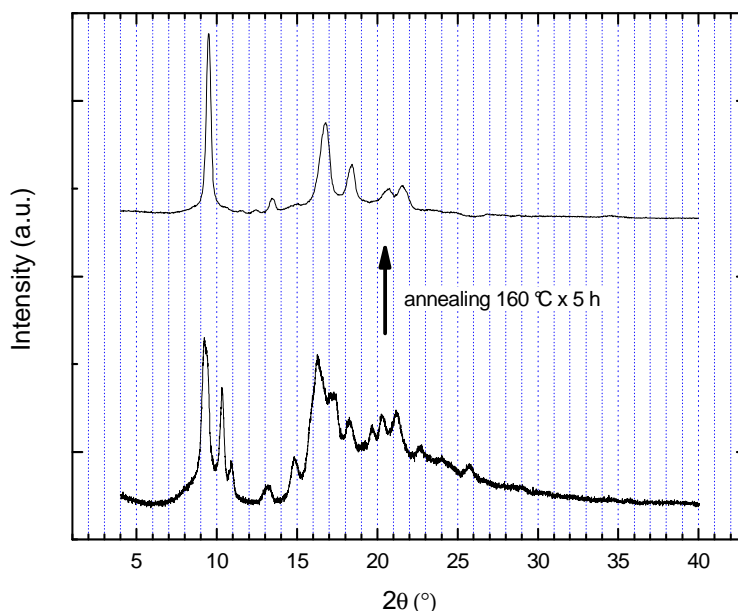

Figure 1.8 X-ray diffraction of the aerogel form II after annealing to 160 °C for 5 hours

It has been reported in a previous work that different i-P4MP1 recrystallization phenomena may occur depending on the CO_2 pressure and on relative contents of solvent and CO_2.[19]

The transition to Form I observed for the Form III gel during CO_2 extraction is not surprising. In fact, the same treatment with supercritical CO_2, when conducted on powders exhibiting Form III (e.g., the fully desiccated decalin gel of Figure 1.3B) leads to the thermodynamically stable form I (Figure 1.9A). This can be easily rationalized by the plasticization of the amorphous phase induced by CO_2, which decreases the glass-transition temperature (Tg ≈ 50-70°C) and hence destabilizes form III that is only kinetically stable.

The supercritical CO_2 treatment on Form IV powders (e.g., the fully desiccated cyclopentane gel of Figure 1.3C) leaves substantially unaltered the diffraction pattern (Figure 1.9B) although we can observe a small increase and a sharpening of the diffraction peak located at $2\theta = 9.4°$ (indicated with an arrow), which could correspond to an increase of the form IV crystals along the direction perpendicular to the 200 plane or to the formation of traces of form I. The complete IV→I transition observed in cyclopentane gels (curve c of Figure 1.6), could be due to a combine effect of the CO_2-induced plasticization and abrupt solvent removal.

15
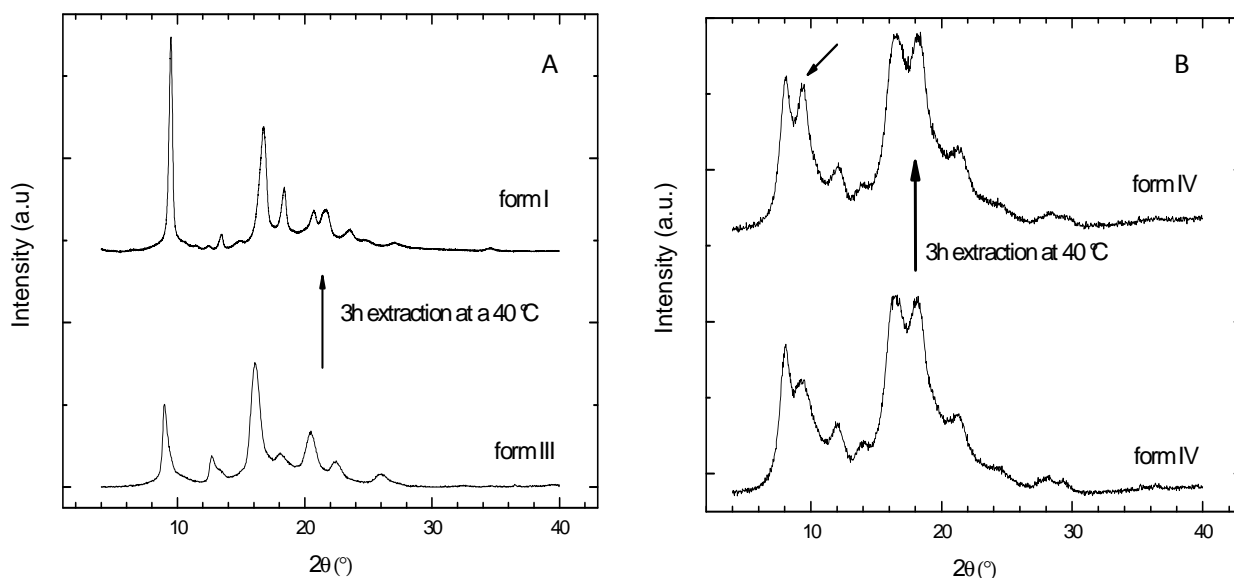
Figure 1.9. *X-ray diffraction patterns of powders exhibiting crystalline Forms III (Figure A) and IV (Figure B), as collected before and after supercritical CO_2 treatment. Form III and Form IV powders were obtained by progressive desorption of solvent in air of gels prepared in decaline (leading to Form III as shown in Figure 1.3B) and CP (leading to Form IV as shown in Figure 1.3C)*

1.4. *Porosity and morphology characterization*

As shown in Figure 1.5, monolithic aerogels can be obtained after solvent extraction with supercritical CO_2. However, depending on the solvent, volume shrinkage may occur during extraction leading to a variation of the aerogel total porosity as shown in row 5 of Table 1.3. It is worth noting that volume shrinkage occurs only with the samples which undergo a crystalline phase transition.

Table 1.3. Crystalline form, degree of crystallinity, total porosity (cm^3g^{-1} and %), surface area S_{BET} (m^2g^{-1}), and pore volumes (cm^3g^{-1}) of i-P4MP1 aerogels obtained by supercritical carbon dioxide treatment of gels prepared at C_{pol} = 20 wt% in different solvents

	1,3,5-trimethylbenzene	decaline	Cyclopentane	cyclohexane
Native gel Crystalline Form	Form I	Form III	Form IV	co-crystal
Aerogel Crystalline Form	Form I	Form I	Form I + Form IV	Form II
Degree of crystallinity (%)	50	50	40	40
Correlation length (nm)	31[a]	26[a]	24[a]	32[b]
Total porosity[c] (cm^3g^{-1}/ %)	6.2/80	4.9/75	2.8/57	2.4/52
S_{BET}[d] (m^2/g)	87	36	31	36
V_{tot}[e] ($cm^3 g^{-1}$)	0.1727	0.0579	0.0745	0.0949
V_{micro}[f] ($cm^3 g^{-1}$)	0.0026	0.0013	0.0018	0.0019

[a] *Correlation length along the direction perpendicular to the Form I (200) plane.*
[b] *Correlation length along the direction perpendicular to the Form II (020) plane*
[c] *Total porosity estimated from the volume/mass ratio expressed as cm^3g^{-1} and % using equation 1.*
[d] *Total area evaluated following the BET model in the standard $0.05 < P/P_0 < 0.25$ pressure range.*
[e] *Pore volume calculated as volume of the liquid at $p/p_0 \approx 0.98$.*
[f] *Micropore volume obtained from the t-plot.*

The scanning electron micrographs (SEM) are reported In figure 1.10 for the different aerogels obtained after CO_2 extraction of gels prepared at C_{pol} = 20 wt% in TMB (Figure 1.10a), decaline (Figure 1.10b), CP (Figure 1.10c) and CE (Figure 1.10d).
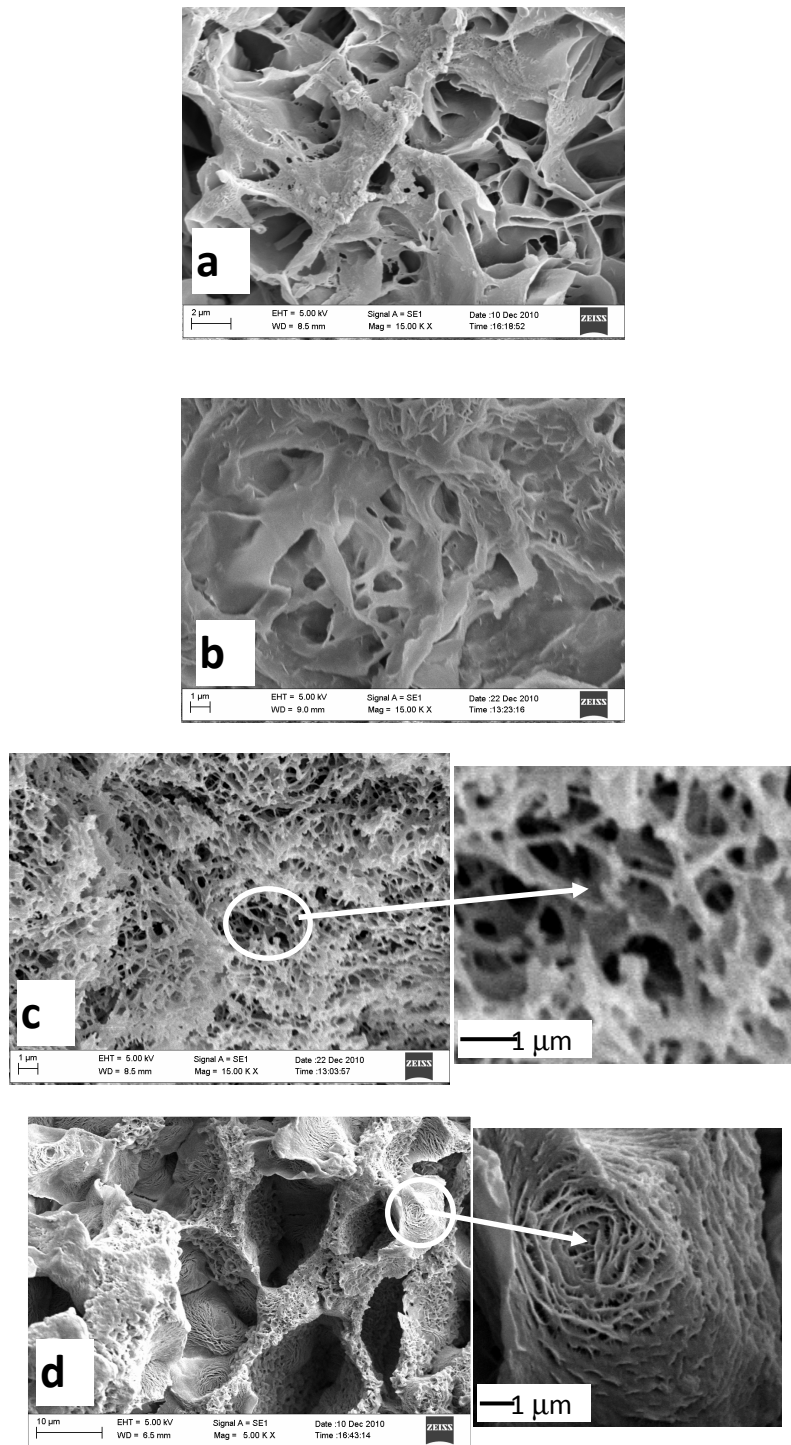
Figure 1.10 *SEM micrographs of aerogels obtained from gels prepared in TMB (a), decaline (b), CP (c) and CE (d) at C_{pol} = 20 wt%. Magnification of aerogels obtained from CP and CE gels are also reported.*

For aerogels obtained from i-P4MP1/TMB and i-P4MP1/decaline gels we can observe a lamellar structure with macropores to about 0.5-4 μm. For the aerogel obtained from CP an open network of fibrils with diameter of c.a. 100 nm with a large number of fiber bundles is observed. Most pores of the network are 0.2-0.5 μm wide.

Finally, for CE aerogels, large honeycomb-type pores with size 8-12 µm are clearly observed while on magnification of the walls smaller macropores with dimensions 0.1 to 0.2µm can be observed between lamellae.

Sorption-desorption N_2 isotherms (where the sorption is expressed as cm^3 of nitrogen in normal conditions (1 atm, 0°C) per gram of polymer) obtained are reported in figura 1.11A. The pore size distributions obtained by applying the NLDFT method are reported in Figure 8B while surface area, pore volume and micropore volume are reported in Table 1.3.
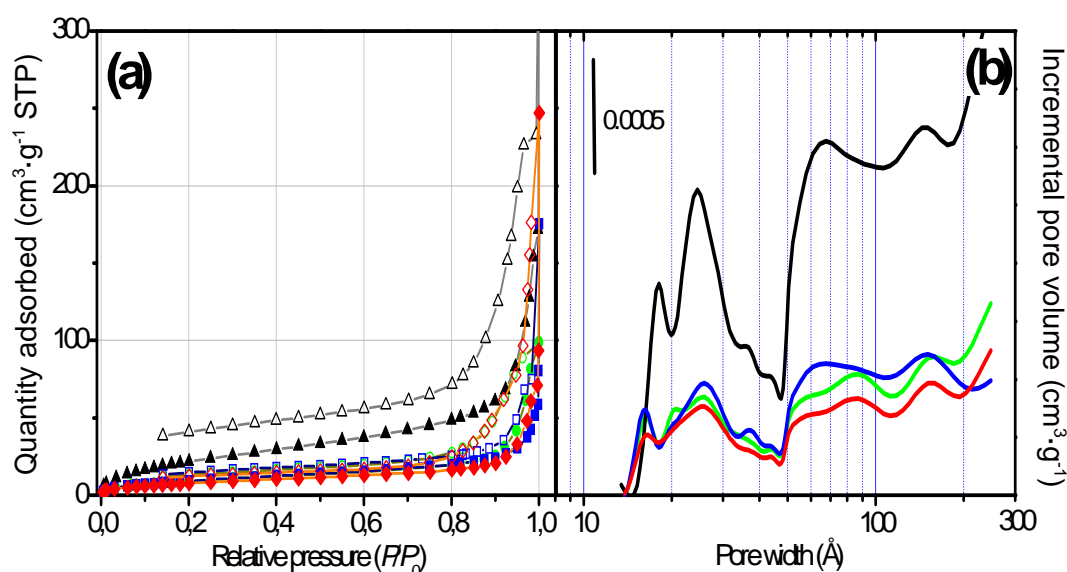

Figure 1.11 *a) Volumetric N_2 adsorption isotherms recorded at 77 K of the aerogels obtained from a 20 wt% gels prepared with CE (circles, green), TMB (triangles, black), decaline (squares, blue) and CP (diamonds, red). Filled and empty scatters refer to the adsorption and desorption branches, respectively. b). Pore distributions obtained by applying the NLDFT method (Non-Local Density Functional Theory, cylindrical pore model, Pillared Clay Surface)[33]*

It is worth noting that N_2 physisorption at 77K allows to characterize only pores in mesopores and micropores range. SEM mesurement (Figure 1.10) have clearly shown the large amount of macropores in this materials: accordingly the pore volumes (V_{totN2}) calculated as volume of the liquid N_2 at $p/p_0 \approx 0.98$ (row 7 of Table 3) differ greatly from the total porosity of the aerogels (row 5 of Table 1.3).

The difference between the total porosity and the V_{totN2} values reported in Table 1.3 then represent an estimate of the macropores volume. In particular, the porosity data of Table 1.3 show that mesoporosity represents only a small fraction of the total porosity (i.e., less than 3%). This agrees with the SEM micrographs of figure 1.9 that show the strong macroporous nature of all specimens.

The shape of the isotherms (type IV and with a large hysteresis loop) indicates the prevalent mesoporous nature of all the specimens and the almost vanishing presence of microporosity. This was confirmed by both the t-plot and the DFT analyses: in fact, if on one hand the t-plot indicates the microporous volume to be less than the 3% of the total pore volume, the distribution of the pores obtained by the DFT method results to be qualitatively very similar for all the aerogels and characterized by a broad and uniform family of pores covering the whole mesopore range (> 20 Å). A small component due to the micropores is present in the range 16-20 Å but is only minoritary. For i-P4MP1/TMB aerogel the persistence of the hysteresis at low p/p_0 values is an indication of the hindered diffusivity of nitrogen due to the monolithic nature of the specimen.

1.5 Concluding remarks

Monolithic aerogels of i-P4MP1 have been obtained by solvent extraction with supercritical carbon dioxide from gels. These aerogels can combine high degrees of porosity with high degrees of crystallinity and exhibit crystalline phases whose nature is determined by the nature of the crystalline cross-link junctions of the native gels.

In particular, the examined gels, whose crosslinking crystalline phases are constituted by a pure polymer form (I, III or IV), present similar polymorphic behavior, as a consequence of solvent removal. In fact, all their native crystalline phases are maintained after slow room temperature desiccation while they are all transformed into the thermodynamically stable form I, after abrupt solvent removal by supercritical carbon dioxide. The examined gels, whose crosslinking crystalline phases are constituted by host-guest co-crystalline forms (with cyclohexane or carbon tetrachloride), also present similar polymorphic behavior as a consequence of solvent removal. However, in this case, the native co-crystalline phases are transformed into form III after slow room temperature desiccation while they are transformed into form II, after abrupt solvent removal by supercritical carbon dioxide.

Scanning electron microscopy has clearly established the macroporosity of the aerogel with large differences in pore size distribution. Thus for the aerogel obtained from P4MP/CE gels, macropores with dimensions larger than 10 μm were observed while for aerogels obtained from P4MP/CP gels most macropores are 0.2-0.5 μm wide.

N_2 porosity measurements have highlighted the absence of microporosity, and particularly the absence of nanoholes arising from solvent extraction from the co-crystalline phase of the gel obtained from CE while for all the areogels the presence of mesopores with a large size heterogeneity have been established.

Finally, it is worth noting that important volume shrinkage have been observed with aerogels obtained from gels, which undergo a crystalline phase transition during the extraction process, specially P4MP/CP and P4MP/CE gels, whereas only Form I gels like those obtained in TMB maintain both the dimension and shape of the native gel. Thus, only Form I gels present a high structural stability necessary to prepare porous P4MP membranes.

REFERENCES

1. Lopez L. C., Wilkes G. L., Stricklen P. M., White S. C., *J. Macromol. Sci.-Rev. Macromol. Chem. Phys.* **1992**, (C32), 301.

2. (a) Skiens W. E., Lipps B. J., Clark M. E., McLain E. A., *J. Biomed. Mater. Res. Symp*. **1971**, (1), 135; (b) Puleo P.K., Paul D. R., Wong P. K. *Polymer* **1989**, (30), 1357.

3. Natta G., Corradini P., Bassi, W. *Rend. Fis. Acc. Lincei* **1955**, (19), 404.

4. Bassi, W., Bonsignori O., Lorenzi G. P., Pino P., Corradini P., Temussi, P. A., *J. Polym. Sci., Polym. Phys. Ed.* **1971**, (9), 193.

5. Kusanagi H., Takase M., Chatani Y., Tadokoro H., *J. Polym. Sci. Polym. Phys. Ed.* **1978**, (16), 31.

6. Charlet G., Delmas G., Revol F. J., Manley R. St. J., *Polymer* **1984**, (25), 1613.

7. Takayanagi M., Kawasaki N., *J. Macromol. Sci. Phys.* **1967**, (B1), 741.

8. De Rosa C., *Macromolecules* **2003**, (36), 6087.

9. Ruan J., Thierry A., Lotz B., *Polymer*, **2006**, (47), 5478.

10. Nakajima A., Hayashi S., Taka T., Utsumi N., *Kolloid. Z. Z. Polym.* **1969**, (234), 1097.

11. De Rosa C., Borriello A., Venditto V., Corradini P., *Macromolecules* **1994**, (27), 3864.

12. De Rosa C., Auriemma F., Borriello A., Corradini P., *Polymer* **1995**, (36), 4723.

13. Hasegawa R., Tanabe Y., Kobayashi M., Tadokoro M., Sawaoka A., Kawai N.. *J. Polym. Sci., Polym. Phys. Ed.* **1970**, (8), 1073.

14. Charlet G., Delmas G., *Polymer Bulletin (Berlin)* **1982**, (6), 367.

15. De Rosa C. *Macromolecules* **1999**, (32), 935.

16. Aharoni S. M., Charlet G., Delmas G., *Macromolecules* **1981**, (14), 1390.

17. Charlet G., Phuong-Nguyen H.; Delmas, G., *Macromolecules* **1984**, (17), 1200.

18. Tanigami T., Suzuki H., Yamaura K., Matsuzawa S., *Macromolecules* **1985**, (18), 2595.

19. Fang J., Kiran E,. *Journal of Supercritical Fluids* **2006,** (38) , 132.

20. Charlet G., Delmas G., *Polymer* **1984**, (25), 1619.

21. Miller R.L., in "Crystallographic Data for Various Polymers" *Polymer Handbook, Third Edition*; John Wiley 1989, VI, 1.

Chapter 2

Nanoporous crystalline phases of Poly(2,6-dimethyl-1,4-phenylene)oxide

2.1 Introduction

Poly(2,6-dimethyl-1,4-phenylene oxide) (PPO) is a well-known engineering thermoplastic that displays excellent thermal and mechanical properties. Its high strength, high heat distortion temperature, chemical resistance, stiffness, and fracture toughness make it a very attractive material.[1,2] However, its brittleness and poor processability have limited its industrial use in a wider range of applications.[3] Major applications of PPO are for automotive, business machine, and electrical/electronics, industries.
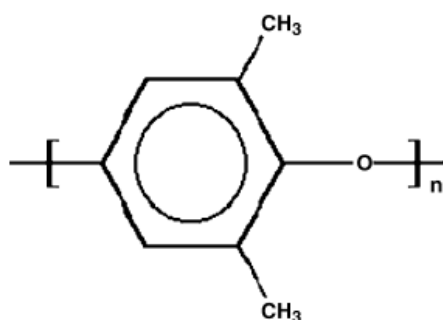
Figure 2.1 Chemical structure of PPO repeating unit

Among many aromatic polymers with high Tg, PPO shows one of the highest gas permeabilities which is attributed to of its well recognized high free volume.[4-6]

Moreover it is resistant against a number of chemical agents, including aqueous solutions of strong acids and bases and therefore is an attractive material for the preparation of membranes. The main interest in the application of unmodified and modified PPO membranes is directed to gas separations[4-7] to reverse osmosis,[8] and in a lesser extent to vapor permeation[9] and pervaporation.[10]

PPO can meet most of the requirements for application in proton exchange membrane fuel cells (PEMFCs) because it is a hydrophobic polymer with high glass transition temperature (Tg =210 °C), high mechanical strength, and excellent hydrolytic stability.[1]

2.2 Characterization of the used commercial PPO

The PPO used in our study was purchased by Sigma Aldrich and presents weight-averaged and number-averaged molecular masses M_w= 59000 g/mol and M_n= 17000 g/mol, respectively.

The PPO X-ray diffraction pattern reported in Figure 2.2 indicates that this commercial sample is semicrystalline.
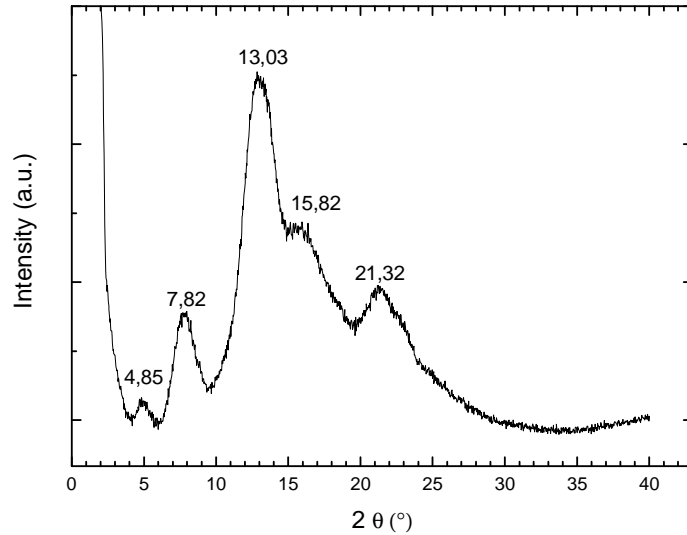

Figure 2.2 X-ray diffraction pattern of commercial PPO

In the figure 2.3 are reported the DSC scans of the commercial semicrystalline sample before (curve A) and after compression molding at 290°C (curve B).
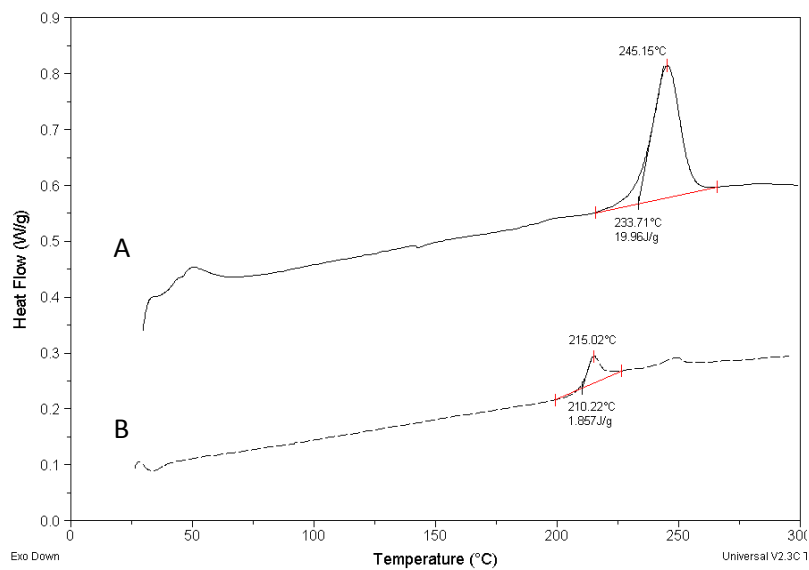

Figure 2.3 DSC of PPO powders: A) commercial semicrystalline sample, B) amorphous sample. Heating rate 10 °C/min

The DSC scan of the commercial PPO shows a melting endotherm peak at c.a. 245 °C while after compression molding at 290°C, the absence of melting peak in the scan B indicates that the sample is totally amorphous and it is possible to observe the glass transition temperature at .c.a 215 °C.

The thermogravimentric analysis of the commercial PPO sample is shown in figure 2.4.
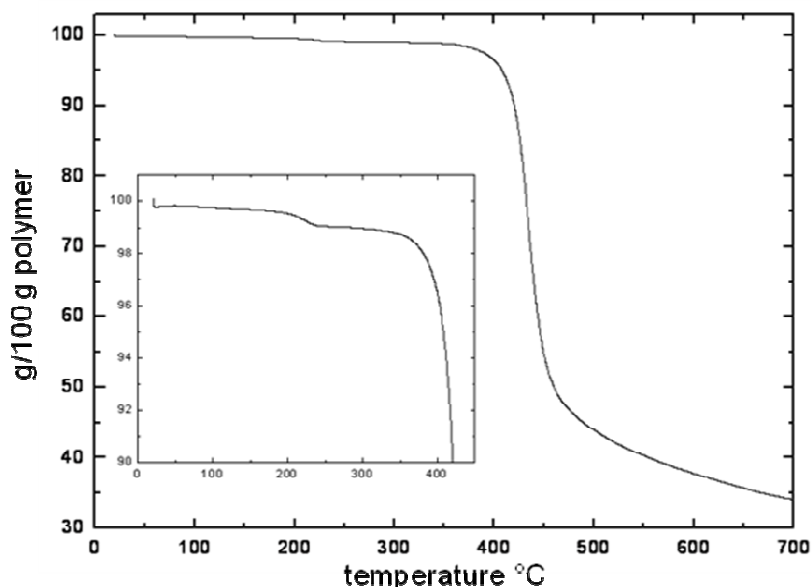
Figure 2.4 TGA of commercial PPO

We can observe that PPO fully degradates in the temperature range 400-500°C, but as can be seen in the inset of the figure, some partial degradation of polymer already starts at about 200°C.

The proximity of the Tg, melting point and degradation temperature produces a poor processability which makes necessary the use of blends with atactic polystyrene to decrease the glass transition and thus the processing temperatures.

2.3 Crystalline phases in PPO thermoreversible gels

2.3.1 Gels with solvents leading to polymer-solvent co-crystalline phases

In the literature several studies showing the key role played by solvent for the PPO crystallization have been reported and the possible formation of co-crystals has been proposed with different solvents.

In particular the existence of a co-crystalline structure has been first proposed with α-pinene and based on the electron and X-ray diffraction measurements, the unit cell parameters have been determined for the PPO/α-pinene co-crystalline structure: $a = b = 11.92$ Å $c = 17.10$ Å.[12]

In Figure 2.5 is shown the X-ray diffraction pattern reported in literature [12] of crystalline PPO obtained from a 1% solution at 100°C after 40 hours of crystallization.
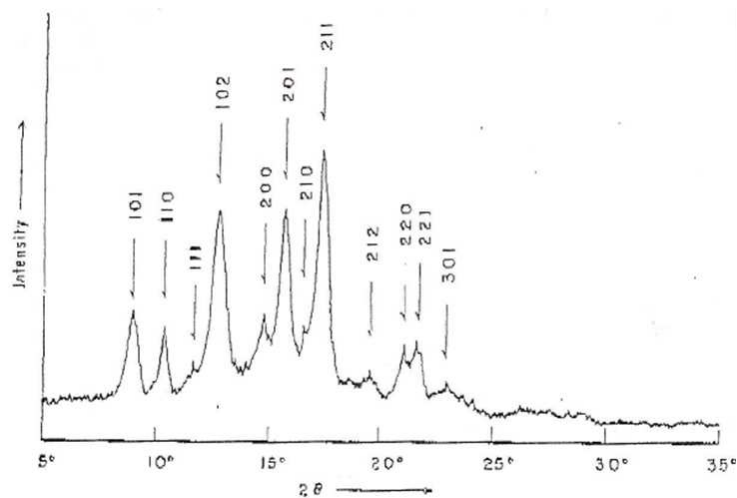
Figure 2.5 *X-ray diffraction pattern of chlatrate structure PPO/α-pinene taken from Horikiri S., Journal of polymer Science **1972**,(10), 1167-70*

Similar diffraction patterns observed for PPO crystals obtained from decalin and tetralin solutions have lead to the conclusion than the similar types of clathrate structures are formed with these two solvents.[13]

In literature the formation of a co-crystal with methylene chloride is also reported but in this case there is a loss of crystallinity during the progressive removal of the solvent.[14]

Thus, PPO gels have been prepared with these three solvents in order to have a better knowledge of PPO gel polymorphism and the crystalline structure of partially and totally desiccated gels have been investigated by X-ray diffraction.

Figure 2.6 shows the X-ray diffraction patterns of the gel prepared in α-pinene at a polymer concentration C_{pol}= 20 wt% collected after progressive desorption of α-pinene in air.
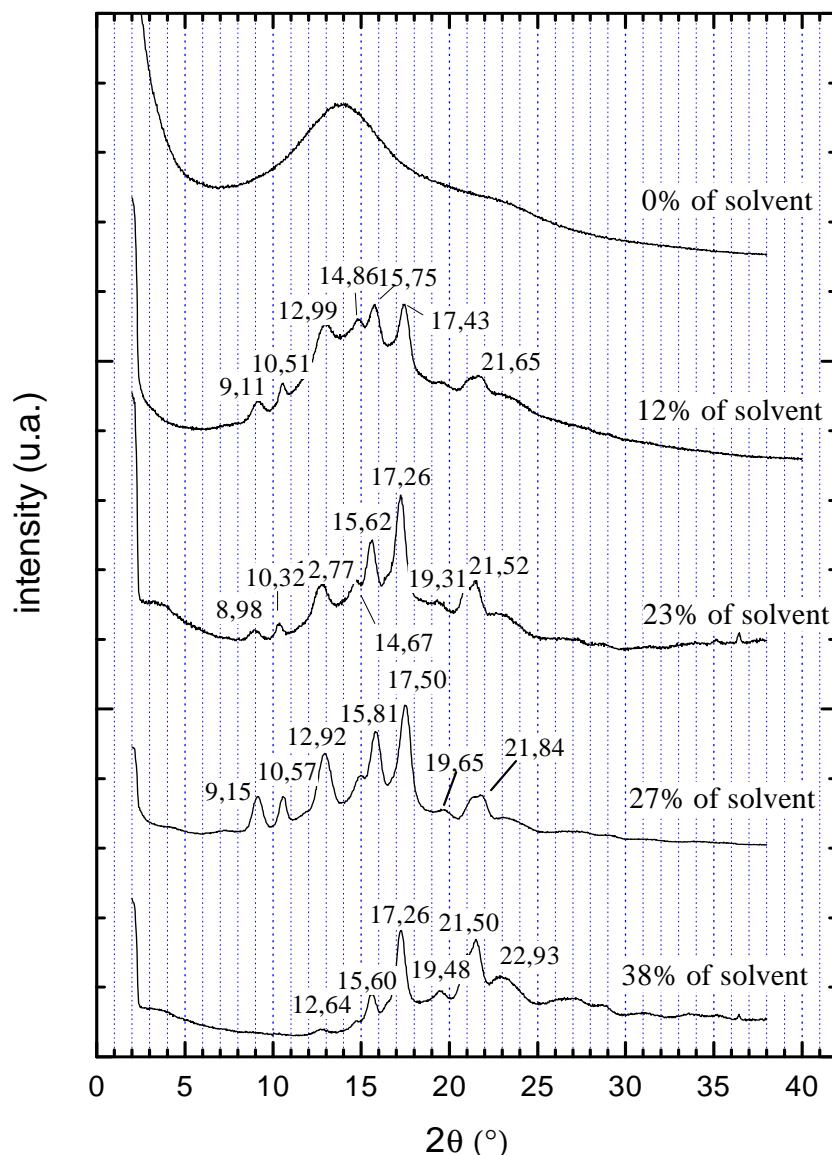
Fig 2.6 *X-ray diffraction patterns of a gel PPO/α-pinene collected during the progressive solvent desorption in air. Concentrations are expressed as solvent weight fraction*

The X-ray diffraction pattern obtained with a partially desiccated gel containing 38 wt% of α-pinene, indicates that, in the native gel, the PPO/α-pinene clathrate crystalline structure is present. However during solvent desorption there is a progressive decrease of the degree of crystallinity, which leads to an amorphous sample.

During this research project, the preparation procedures, thermal properties, polymorphic behavior and crystal structure of co-crystalline phase of PPO with α-pinene have been deeply characterized and detailed results are reported in Chapter 3.

X-ray diffraction patterns of partially desiccated PPO/tetralin and PPO/decalin gels obatined by solvent evaporation in air are reported in Figures 2.7A and 2.7 B, respectively.
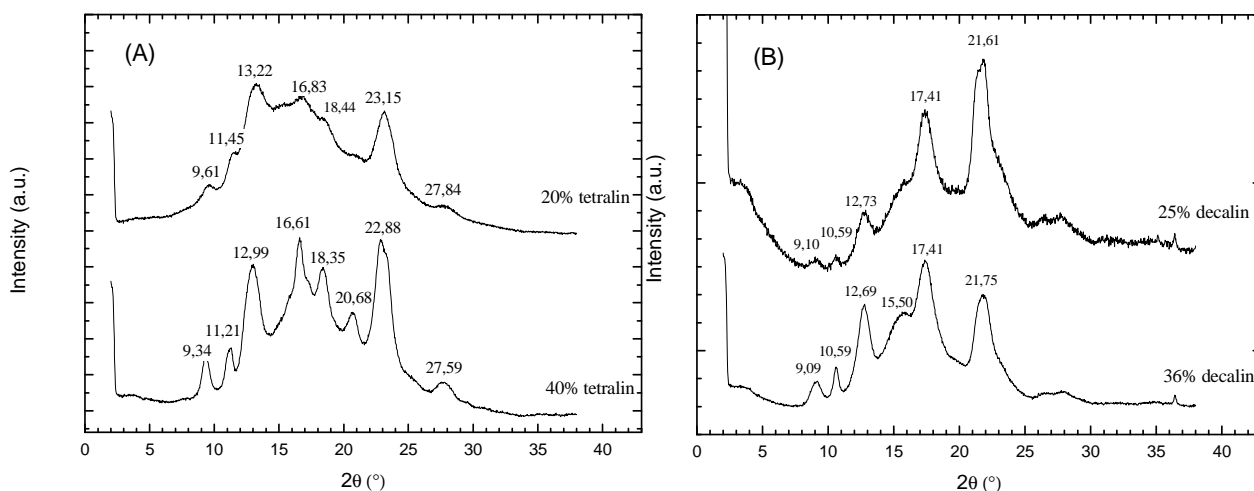
Fig 2.7 *X-ray diffraction patterns of partially desiccated PPO/tetralin (A) and PPO/decalin (B) gels collected during progressive solvent desorption in air. Concentrations are expressed as solvent weight fraction.*

We can observe that, as already reported in the literature, diffraction patterns similar to the one obtained for the PPO gel obtained with α-pinene, are obtained with PPO/tetralin and PPO/decalin gels. This result suggests that a similar clathrate structure is formed in the gels obtained with these three solvents.

We can also observe that, as with α-pinene, a progressive amorphization occurs during tetralin and decalin evaporation in air.

2.3.2 Gels with other solvents

The crystalline structure obtained with solvents which are not listed in the litterature among those leading to the formation of a co-crystalline phase has been also investigated and the X-ray diffraction patterns of partially desiccated PPO/CCl₄ in gels are reported in Figure 2.8.
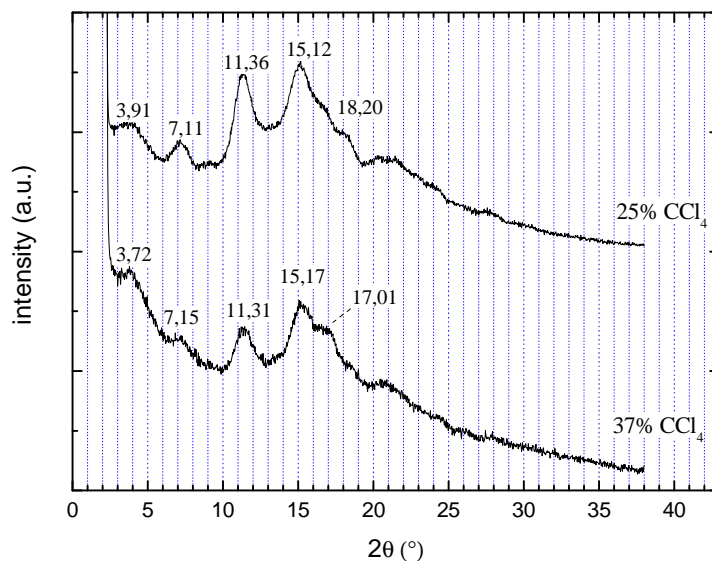
Figure 2.8 *X-ray diffraction patterns of partially desiccated PPO/CCl₄ gels collected during solvent desorption in air. Concentrations are expressed as solvent weight fraction*

The X-ray diffraction patterns reported in Figure 2.8 clearly show that in PPO/CCl$_4$ gels a crystalline structure totally different to the PPO/α-pinene clathrate is obtained.

2.4. Crystalline structure in samples obtained from PPO/gels after complete solvent removal in supercritical conditions

It has been shown for syndiotactic polystyrene co-crystalline phases that complete solvent removal from the co-crystalline phase can be achieved with supercritical carbon dioxide and the nanoporous δ or ε crystalline phase are obtained.[15]

Thus, the solvent extraction with supercritical CO$_2$ was also applied to PPO gels obtained with the three solvents leading to the formation of a co-crystalline phase (i.e. α-pinene, tetralin and decalin) but also with other solvents such as carbon tetrachloride, 1,2,4-trichlorobenzene, 1-chlorodecane, 1.2-dichloroethane, benzene, 1,4-dimethylnaphthalene, and dichloromethane.

The X-ray diffraction patterns of powder samples as obtained by PPO gels prepared in different solvents after complete solvent removal with supercritical CO$_2$ are reported in Figure 2.9.
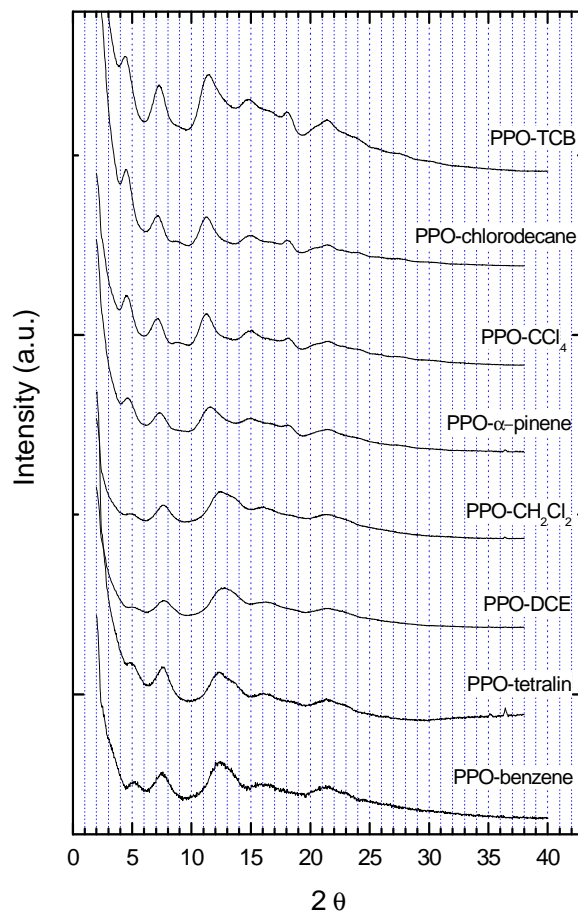
Fig 2.9 *X-ray diffraction patterns of gels extract in supercritical CO$_2$*

We can observe that for all the solvents apart from decalin which leads to a fully amorphous sample, highly crystalline samples are obtained from PPO gels after solvent removal with supercritical CO$_2$. The x-ray diffraction patterns present peaks being located at definitely different angles and the diffraction angle (2θ) and Bragg distances (d) values of the second and third peak of each pattern are as listed in Table 2.1.

For instance, we can note that the value of the second peak 2θ change from a minimum value of 7.11 (obtained with chlorodecane) to a maximum value of 7.63 (obtained with benzene). The d values obtained with the different solvents clearly show that the solvent plays a fundamental role in determining the periodicity of the final crystalline phase.

Table 2.1 *Diffraction angle (2θ) and Bragg distances (d) values of the second and the third reflections observed in the X–ray diffraction patterns of PPO semi-crystalline powders of Figure 2.10 obtained by complete solvent extraction from gels with supercritical CO$_2$.*

PPO from benzene gels			PPO from tetralin gels			PPO from CH$_2$Cl$_2$ gels			PPO from DCE gels			PPO from α-pinene gels			PPO from TCB gels			PPO from CCl4 gels			PPO from chlorodecane gels		
2θ (deg)	d (nm)	I	2θ (deg)	d (nm)	I	2θ (deg)	d (nm)	I	2θ (deg)	d (nm)	I	2θ (deg)	d (nm)	I	2θ (deg)	d (nm)	I	2θ (deg)	d (nm)	I	2θ (deg)	d (nm)	I
5.15	1.70	m	4.95	1.80	w	4.75	1.85	w	4.85	1.80	w	4.70	1.90	w	4.35	2.05	m	4.55	1.95	s	4.45	2.00	m
7.65	1.15	s	7.65	1.15	s	7.70	1.15	s	7.55	1.10	s	7.30	1.20	s	7.35	1.20	s	7.15	1.25	s	7.20	1.20	s
																		9.0	1.05	vw	9.0	1.05	vw
12.5	0.70	vs	12.5	0.70	vs	12.5	0.70	s	12.5	0.70	s	11.5	0.75	s	11.5	0.75	vs	11.0	0.80	vs	11.0	0.80	vs
16.0	0.55	vw	16.0	0.55	vw	16.0	0.55	vw	16.0	0.55	w	15.0	0.60	w	15.0	0.60	m	15.0	0.60	m	15.0	0.60	m
									18.5	0.50	vw	18.0	0.50	w	18.0	0.50	w	18.0	0.50	w	18.0	0.50	w
																		20.5	0.45	vw	20.5	0.45	vw
21.5	0,40	vw	21.5	0.40	vw	21.5	0.40	vw	21.5	0.40	vw	21.5	0.40	w	21.5	0.40	m	21.5	0.40	w	21.5	0.40	w

The whole set of the data of Figure 2.9 and Table 2.1, indicates that the solvent plays a fundamental role in determining the periodicity for the final crystalline phase and PPO can crystallize in markedly different crystalline modifications. Additional results indicate that there is nearly a continuum of crystalline phases between two limit structures exhibiting highest and lowest 2θ values. In fact, for instance, powders from gels subjected to complete solvent removal present a progressive shift of the diffraction peaks to lower 2θ values, along the sequence benzene $\approx$ tetralin > methylene chloride> 1,2-dichloroethane > α-pinene> trichlorobenzene> chlorodecane $\approx$ CCl_4.

2.5 Solvent induced crystallization of amorphous PPO

The structural characterizations reported in the prevoius sections focussed on semi-crystalline samples obtained from gel samples prepared in concentrated polymer-solvent solutions. However semicrystalline PPO samples can also be obtained by solvent induced crystallization of amorphous PPO. In particular crystallization of amorphous PPO can by achieved with several solvent by immersion in pure liquid or exposure to vapors.

The X-ray diffraction patterns of an amorphous PPO film before and after exposure to benzene (RT, 4 hours), chlorobenzene (RT, 15 hours), and carbon tetrachloride (T $=80°C$, 5 hours) vapors and solvent removal with supercritical CO_2 are reported in Figure 2.10.
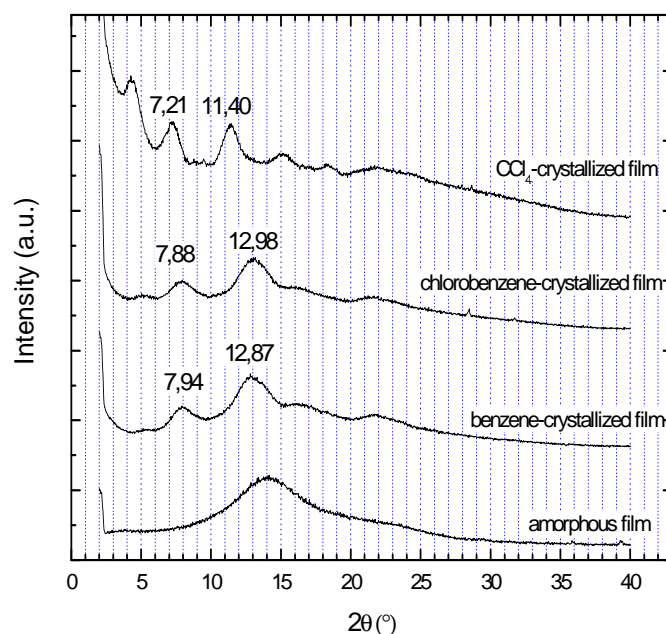

Figure 2.10 *X-ray diffraction patterns of amorphous PPO before and after exposure to vapors of benzene, chlorobenzene and CCl4 followed by* solvent removal with supercritical CO_2

We can note that as for samples obtained from PPO gels, the crystalline structure obtained by solvent-induced-crystallization fo amorphous PPO depends on the solvent. Moreover it is worth emphasizing that, as in the gel, the sample crystalizzed with CCl_4 presents 2θ values of the second and third peak at about 7.20 and 11.40.

The crystallization of amorphous PPO with a solvent forming a co-crystalline phase has been also investigated and the X-ray diffraction patterns of a partially desiccated PPO/decalin gel and of an amorphous film immerged in decalin at 110 °C for 3 h are reported in Figure 2.11.
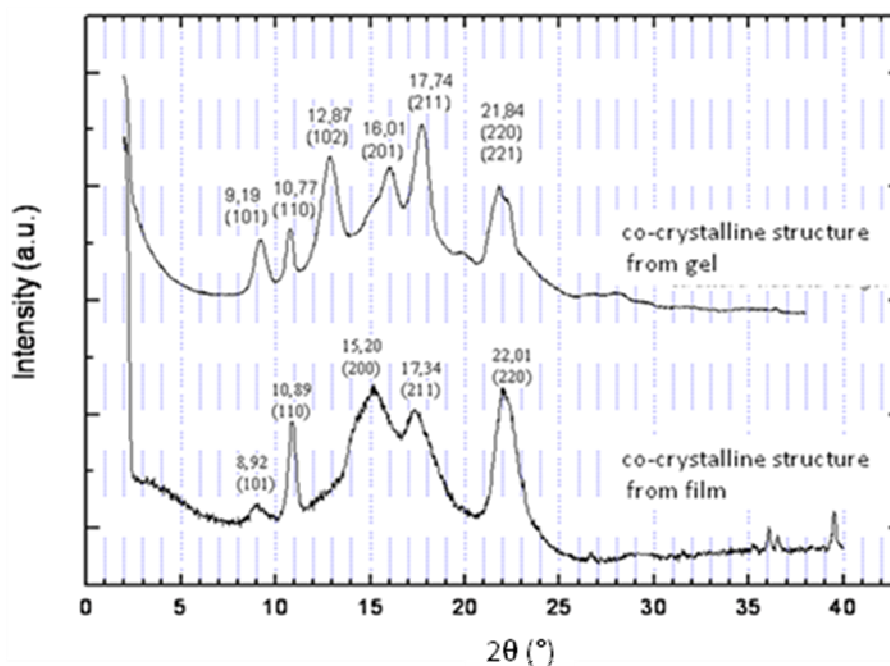
Figure 2.11 X-ray diffraction patterns of a partially desiccated decalin gel and of an amorphous PPO film immerged in decalin

We can observe that a co-crystalline phase can be obtained by solvent-induced crystallization of amorphous PPO. However, variations in the x-ray diffraction patterns indicate that differences in the structural organization in both samples. In particular, for the clathrate phase obtained from the amorphous PPO film, the diffraction peaks at $2\theta = 10. 9$ and 22.0 corresponding to the 110 and 220 crystallographic planes are very intense and very narrow while for the clathrate obtained in the gel these these peaks are less intense. The greater intensity of the peaks with k=0 indicates that in the film the crystals present a partial (110) uniplanar orientation.

The possible formation of the typical clathrate structure from a non-clathrate semi-crystalline PPO has been also investigated and in Figure 2.12 are reported the X-ray diffraction patterns of benzene-crystallized film (such as the one reported in Figure 2.10) before (curve A) and after (curve B) immersion in decalin for 3 hours at 110 °C.

33

Figure 2.12 *X-ray diffraction patterns of a film crystallized in benzene before (curve A) and after(curve B) immersion in decalin at 112 °C for 3 hours*
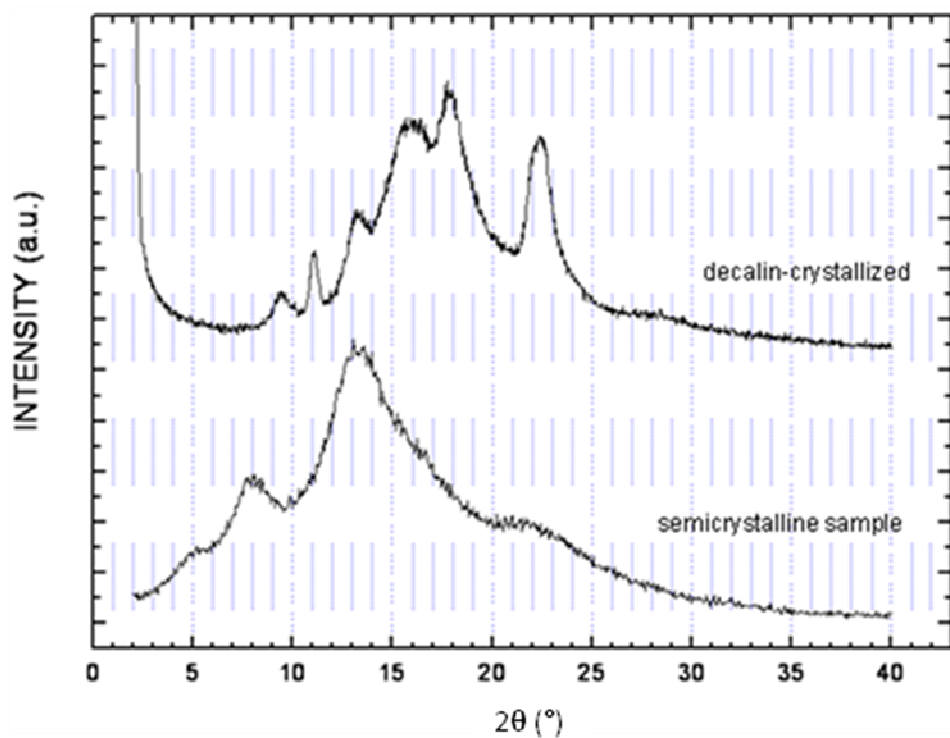
The amount of decalin absorbed during the treament is c.a. 37 wt% and the x-ray diffraction patterns of Figure 2.12 clearly show a change of the crystalline structure and the formation of the typical PPO clathrate structure.

2.6 SORPTION PROPERTIES OF PPO

2.6.1 Nitrogen sorption

Volumetric nitrogen adsorption measurements at 77°K have is a been carried out in order to assess the presence of microporosity in PPO samples obtained after supercritical CO_2 extraction of the solvent from PPO gels.

The N_2 isotherms obtained for semicrystalline PPO powders obtained by CO_2 supercritical extraction of gels prepared in benzene and CCl_4, amorphous powder obtained by CO_2 supercritical extraction of a gel prepared in decalin and an amorphous film obtained by compression molding are compared in Figure 2.13. The total surface area evaluated following the BET model, total pore volume and micropore volume are reported in table 2.2.

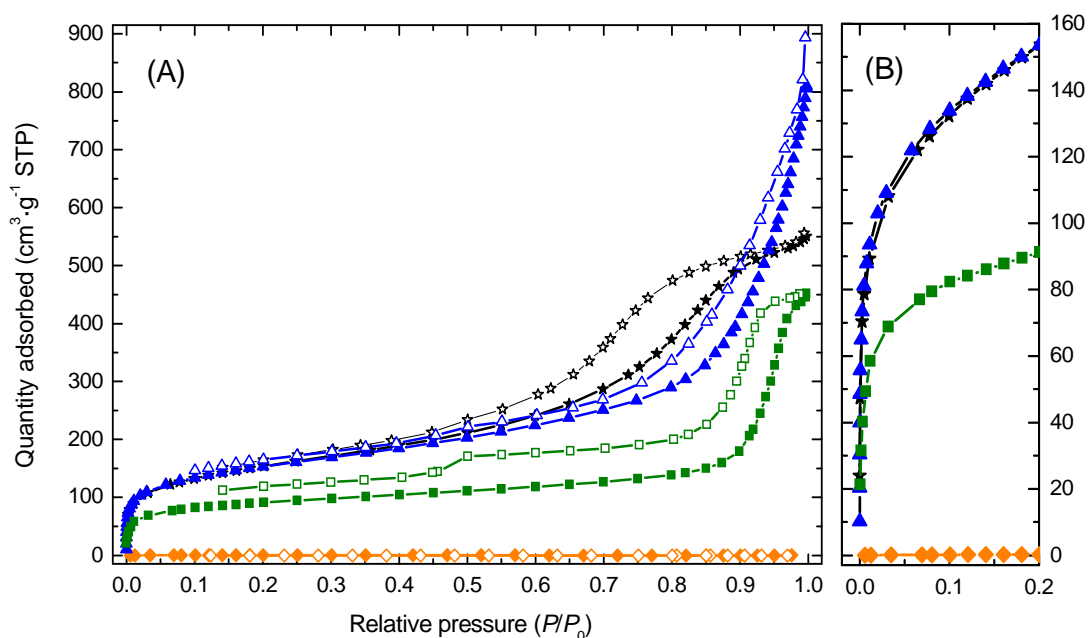***Figure 2.13*** *a) Volumetric N_2 adsorption isotherms recorded at 77 K on the amorphous powder PPO (square, olive), amorphous PPO by compression molding film (diamonds, orange), PO/benzene (stars, black) and PPO/CCl$_4$ (triangle, blue). Filled and empty scatters refer to the adsorption and desorption branches, respectively. b) shows the detail of the adsorption branch reported in A, for low pressure.*

Table 2.2 *Surface area (m^2 g^{-1}), and pore volume (cm^3 g^{-1}) of PPO samples.*

	S_{BET}[a]	S_{micro}[a]	V_{tot}[b]	V_{micro}[c]
semicrystalline PPO from gel with CCl$_4$	549	214	0.99	0.12
semicrystalline PPO from gel with benzene	552	171	0.82	0.10
amorphous PPO from gel with decalin	320	102	0.63	0.06
Amorphous PPO by compression moulding	0.76	-	0	-

[a]Total surface area evaluated following the BET model in the standard $0.05 < P/P_0 < 0.25$ pressure range.

[b]Total pore volume calculated as volume of the liquid at $p/p_0 \approx 0.90$.

[c]Micropore volume obtained from the t-plot.

The values reported in Table 2.2 show that the amorphous sample obtained by compression molding do not present any porosity while all the other samples obtained by CO$_2$ supercritical extraction of gels prepared in benzene, CCl$_4$, and decalin are highly porous with large surface area and pore volume values. It is also worth noting that microporosity account to about the 30% of the total surface area.

Particularly impressive is the result that both semicrystalline samples possess porosity and microporosity nearly double that of the amorphous sample obtained from the decalin gel. This result clearly indicate that the crystalline phases obtained after solvent removal are nanoporous.

2.6.2 Sorption of volatile organic compounds

Particularly relevant molecular separations are those implying the removal of volatile organic compounds (VOC) from water and air. In particular, it has been observed for the case of syndiotatactic polystyrene that nanoporous-crystalline polymeric phases are extremely suitable because they are able to include non polar molecules, as guest of their crystalline cavities, and to exclude the highly polar water molecules.

Thus, the sorption properties of VOC from diluted aqueous solutions and vapor phase at low activity in PPO nanoporous crystalline phases have been investigated and compared to amorphous PPO samples.

i) Sorption of benzene from diluted aqueous solution

The FTIR spectra of PPO films after equilibrium sorption of benzene, from a 10 ppm aqueous solution at room temperature, are compared in figure 2.14 for an amorphous film obtained by compression molding and for the CCl_4-crystallized PPO film.
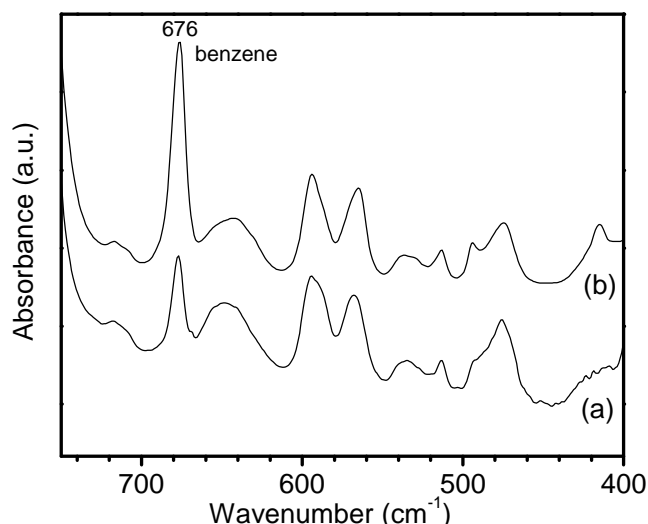

Figure 2.14 *FTIR spectra in the wavenumber range 750-400 cm^{-1} of PPO films after equilibrium benzene sorption from 10 ppm aqueous solutions: (a) amorphous; (b) CCl$_4$–crystallized.*

From the intensity of the benzene peaks, like that one at 676 cm^{-1}, it is immediately apparent that the benzene sorption from the semicrystalline film is nearly triple than for the amorphous film. A gravimetric calibration curve allows establishing that the equilibrium benzene sorption in the semicrystalline sample is close to 10 wt %. This benzene uptake corresponds to a concentration increase of 10 000 times and is also more than double than from an s-PS sample exhibiting the nanoporous δ phase.

The higher benzene uptake obtained with the crystalline PPO sample clearly indicate that the crystalline phase is nanoporous.

ii)Sorption of 1,2-dichloroethane from diluite aqueous solution

In several works[15], the sorption of 1,2-dichloroethane (DCE) from diluted aqueous solutions and from vapor phase in the syndiotactic polystyrene nanoporous phases has been investigated. This choice of DCE, was motivated by is the additional information, which comes from its conformational equilibrium. In fact because essentially only its trans conformer is included into the s-PS clathrate phase while both trans and gauche conformers are included in the amorphous phase, quantitative evaluations of vibrational peaks associated with these conformers allow to evaluate the

amounts of DCE confined as guest in the clathrate phase or simply absorbed in the amorphous phase.[17]

The choice of DCE was also motivated by its presence in contaminated aquifers and by its resistance to remediation techniques based on reactive barriers containing Fe^0.[18]

Thus, in order to make a comparison with s-PS, the sorption of DCE from diluted aqueous solutions was also investigated for amorphous and semi-crystalline PPO films.

In Figure 2.15, are compared, the DCE equilibrium uptakes from diluted aqueous solutions, as obtained by FTIR measurements, for s-PS samples with the nanoporous δ form and the non-porous γ form and for PPO samples. For the sake of comparison, equilibrium sorption capacity of DCE from activated carbon is also shown.[19]
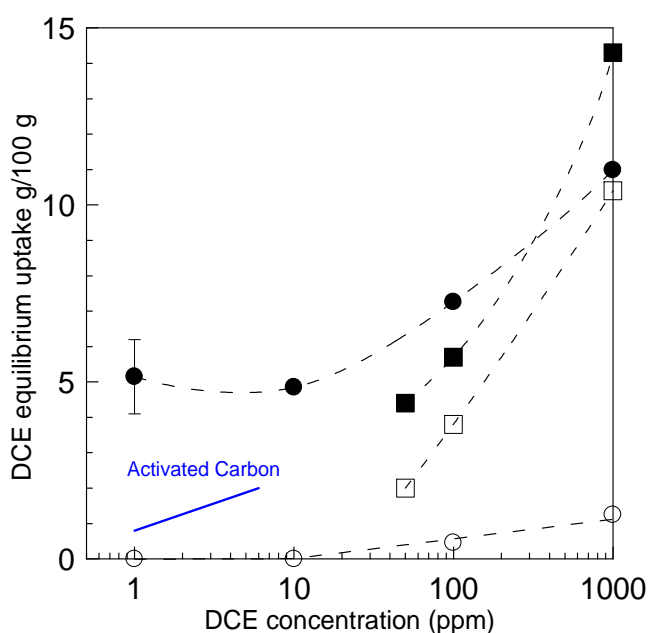
Figure 2.15 *1,2-dichloroethane equilibrium sorption at room temperature from water, as a function of its concentration in polymer samples: (filled symbols) including nanoporous crystalline phases; (empty symbols) absorbing guest molecules only in amorphous phases. Circles correspond to s-PS samples (δ and γ form aerogels) while squares correspond to PPO samples (nanoporous-crystalline and amorphous powders).*

It is clearly apparent that samples including nanoporous crystalline phases (δ for s-PS and crystallized by benzene for PPO) present higher guest solubility than samples absorbing DCE only in the amorphous phase (γ for s-PS and amorphous for PPO).

As for s-PS, for low pollutant concentration, the DCE sorption occurs essentially only in the crystalline phase. In particular, for the most diluted aqueous solution (1 ppm), the sorption capacity is larger than 5 $g_{DCE}/100g_{polymer}$, i.e. leads to a concentration increase of 50000 times. As for PPO, the DCE uptake from the amorphous sample is remarkable, as expected on the basis of its well recognized high free volume.[5-7] However, the sorption from the semicrystalline sample is definitely higher than for the corresponding amorphous phase and, in particular for 50 ppm solutions, the sorption capacity of the semicrystalline sample is more than double than for the amorphous sample.

iii) Sorption of benzene and carbon tetrachloride vapors at low activity

The sorption experiments of benzene and carbon tetrachloride vapors at low activity were performed using a amorphous PPO sample obtained by supercritical CO_2 extraction of a gel with decalin and two semi-crystalline samples obtained by extraction with supercritical CO_2 of gels with benzene and CCl_4, whose X-ray diffraction patterns are shown in figure 2.9. These semicrystalline samples were chosen because they represent the two limit structures exhibiting highest and lowest 2θ values as previously reported in Table 2.1.

Benzene and CCl_4 gravimetric sorption isotherms at 35°C and pressures lower than 0.08 P/P$_0$ are reported in Figure 2.16A and 2.16B, respectively. For the sake of comparison the benzen uptake from a δ nanoporous crystalline powder of s-PS with degree of crystallinity close to 30% is also shown in Figure 2.16A.
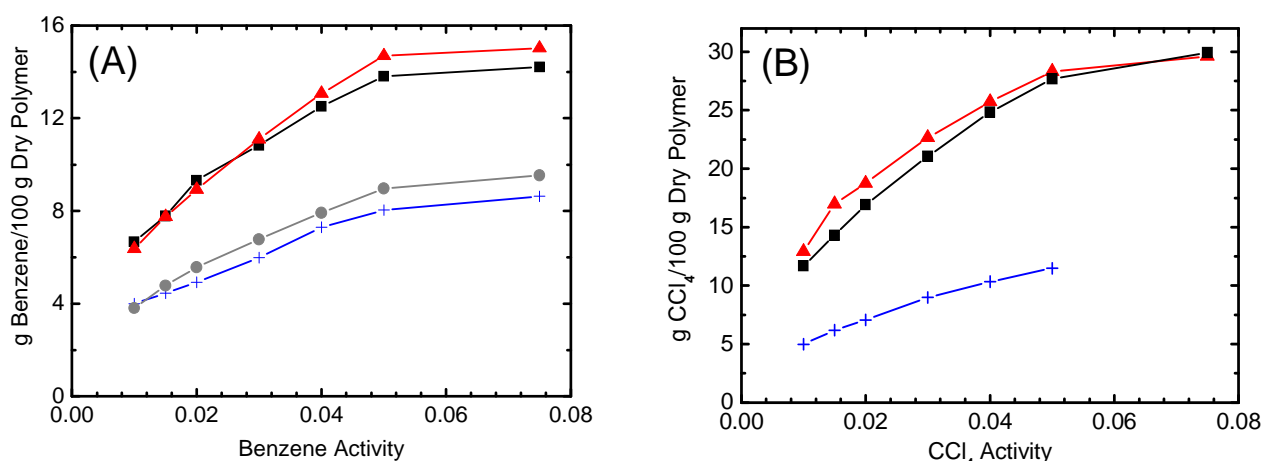

Figure 2.16 *Benzene (A) and CCl$_4$ (B) gravimetric sorption isotherms, at 35°C and at pressures lower than 0.08 P/P$_0$, on PPO samples: amorphous (**+**); benzene-crystallized (■) and CCl$_4$– crystallized (▲).Benzene uptake from an s-PS powder exhibiting the δ nanoporous crystalline phase (●)*

It is clearly apparent that large solvent uptakes occur for all PPO samples already at very low solvent activities, clearly confirming the presence of nanopores (microporosity). However, the lowest solvent equilibrium uptakes occur for the amorphous powder while the guest uptake of the two highly crystalline PPO powders is roughly double with respect to those of the amorphous powder. This results clearly indicates the nanoporosity of the PPO crystalline phases.It is also worth noting that the VOC uptake in semi-crystalline PPO samples is much higher than for the δ form (nanoporous) s-PS.

It is worth noting that the two highly semicrystalline powders obtained from benzene and CCl_4 gels, although exhibiting the two limit crystalline structures of Figure 2.9 present very similar and maximum vapor uptake.

As the crystalline phase constitutes roughly only 30% of the semicrystalline powders, the data of Figure 2.16A and B indicate that the PPO crystalline forms present a guest solubility much higher than for the (also nanoporous) PPO amorphous phase.

For instance, for $P/P_0 = 0.075$, the benzene uptake is 15 wt% for the semicrystalline sample (19 wt% as calculated for the crystalline phase) while it is 8.5 wt% for the fully amorphous sample. This guest solubility difference between amorphous and crystalline phases is higher for CCl_4. At $P/P_0 = 0.075$ the uptake is nearly 13 wt% for amorphous PPO, higher for the highly crystalline powder (30 wt%) and is calculated to be very high for the nanoporous crystalline phase (41 wt%). It is also worth adding that although this weight uptake of the two guests in the crystalline phase is widely different, the corresponding molar uptake is similar, i.e., for $P/P_0 = 0.075$, not far from 1 guest molecule per 3 monomeric units.

2.7. Thermal stability of PPO nanoporous crystalline structure

A preliminary study of the thermal stability of PPO nanoporous crystalline structures has been conducted and in figure 2.17 the X-ray diffraction patterns of a nanoporous PPO film obtained by crystallization with benzene of an amorphous sample are reported for different annealing temperatures.
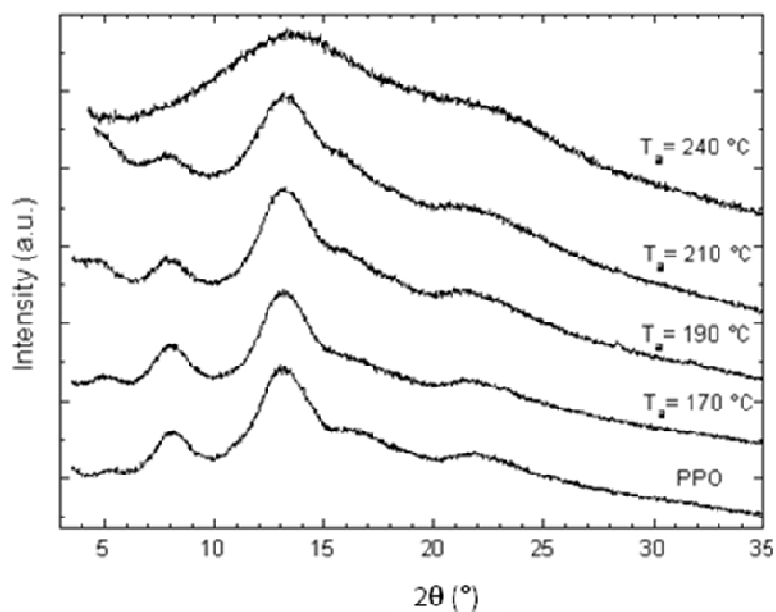
Figure 2.17 *X-ray diffraction patterns of a semicrystalline nanoporous PPO obtained by crystallization of amorphous PPO with benzene annealed at various temperatures*

The diffraction patterns show that by increasing the annealing temperature up to 210°C the degree of crystallinity remain unaltered and after annealing at 240°C a totally amorphous sample is obtained.

The PPO nanoporous crystalline form is much more stable than the syndiotactic δ and ε nanoporous crystalline forms for which a loss of crystalline nanoporosity due to transition, toward the γ phase occurs at nearly 100 °C.

2.8 CONCLUDING REMARKS

The PPO is a polymer soluble in many organic solvents and it has been taken advantage of this property to prepare several gels , also aiming to study the polymorphism and the nanoporous forms.

The formation of highly crystalline or fully amorphous PPO powders can be obtained by solvent removal from gels, by making suitable selection of the solvent. Moreover, the choice of the gel solvent allows controlling the nature of the crystalline phase. In particular, X-ray diffraction patterns indicate the presence of many (if not a continuum of) modifications between two limit ones, exhibiting diffraction peaks at lowest or highest angles.

Similar crystalline phases, although generally exhibiting lower degrees of crystallinity, can be also obtained by solvent induced crystallization in amorphous and crystalline films.

As widely recognized, amorphous PPO is a high free volume, ultrapermeable phase, which exhibits very high guest solubility, already for low guest activity. Surprisingly, the semicrystalline PPO samples present a much higher solubility of many guests (e.g., benzene, CCl_4). These sorption results, as well as density measurements and classical BET experiments, clearly indicate that the PPO crystalline phases are nanoporous.

The nanoporous nature of these crystalline phases has been also confirmed by density measurements by flotation of film samples. In fact, the density of the benzene-crystallized PPO semicrystalline film (1,009 ±0,002 g/cm^3) is lower than the density of fully amorphous PPO films (1,016 ± 0,004 g/cm^3). These data, by assuming a degree of crystallinity of 30%, as evaluated from the X-ray diffraction pattern of figure 2.18, allow predicting a density of the crystalline phase of roughly 0.99 g/cm^3.

Applications of polymeric nanoporous crystalline phases, till now only based on s-PS, are expected to be widely expanded in the near future. In fact, many applications are predictable for PPO nanoporous crystalline phases, which present with respect to nanoporous crystalline phases of s-PS the advantage of faster guest sorption kinetics, due to the nanoporous nature also of the amorphous phase, as well as the advantage of higher thermal stability.

Finally, the clathrate structures found in diluited solutions of decalin, tetralin, and α-pinene, which have been reported in the literature, have turned our attention to the study of the gel obtained with these solvents. In particular, it has been shown that clathrate structures can be also obtained in PPO gels but also by crystallization of amorphous PPO. After solvent removal in supercritical conditions, these clathrate structures with the exception of decalin which gives a fully amorphous sample, gives nanoporous crystalline forms similar to the ones obtained with the other solvents. In

the next chapter the characterization of the co-crystalline phase of PPO with α-pinene will discussed.

References

1. Hay A.S., J *Polym Sci Part A*, **1998**, (36), 505.

2. Wang X., Feng W., Li H., Ruckenstein E., *Polymer*, **2002**, (43), 37.

3. Puskas J.E., Kwon Y., Alstadt V., Kontopoulou M., *Polymer*, **2007,** (48), 590.

4. Alentiev A., Drioli E., Golemme M., Olinich O., Lapkin A., Volkow V., Yamobolski Yu., *Journal of Membrane Science*, **1998**, (138), 99.

5. Ilinitch O., M., Fenelonov V. B., Lapkin A. A., Okkel L. G., Terskikh V. V., Zamaraev K. I., *Microporous Mesoporous Materials,* **1999**, (31), 97.

6. Khulbe K.C., Matsuura T., Lamarche G., Lamarche A.-M., *Journal of Membrane Science,* **2000**, (170), 81.

7. a) Bauer C. J. M., Smid J., Olijslager J., Smolders C. A., *Journal of Membrane Science*, **1991**, (57), 307; b) Smid J., Albers J. H. M., Kusters A. P. M., *Journal of Membrane Science*, **1991**, (64), 121; c) Fu H., Jia L., Xu J., *Journal of Applied Polymer Science,* **1994**, (51), 1405; d) Polotski E. A., Polotskaya G. A., *Journal of Membrane Science*, **1998**, (140), 97.

8. a) Huang R Y. M., Kim J. J., *Journal of Applied Polymer Science*, **1984**, (29), 4017; b) Hamza A., Chowdhury G., Matsuura T., Sourirajan S., *Journal of Applied Polymer Science*, **1995**, (58), 613; c) Hamza A., Chowdhury G., Matsuura T., Sourirajan S., *Journal of Membrane Science*, **1997**, (129), 55.

9. Fu H., Jia L., Xu J., *Journal of Applied Polymer Science*, **1994**, (51), 1405.

10. a) Mulder M. H. V., Oude-Hendrikman J., Wijmans J. G., Smolders C. A., *Journal of Applied Polymer Science,* **1985**, (30), 2805; b) Schauer J., Schwarz H. H., Eisold C., *Angew Makromol Chem*, **1993**, (206), 193.

11. a) Liska J, Borsig E., *Chem. Listy,* **1992,** (86), 900; b) Liska J., Borsig E., *Journal of Macromolecular Science, Rev Macromol Chem Phys*, **1995**, (C35), 517.

12. Horikiri S.*, Journal of polymer Science,* **1972,** (10), 1167.

13. Hurek J., Turska E., *Acta Polymerica*, **1984,** (35), 201.

14. Factor A, Heinsohn G. E., Vogt Jr. L. H., *Polymer Letters*, **1969**, (7), 205.

15. a)Reverchon E., Guerra G., Venditto V., *Journal of Applied Polymer Science* **1999**, (74), 2077; b) Ma W., Yu J., He J., *Macromolecules* **2005**, (38), 4755.

16. (a) Albunia A.R., Di Masi S., Rizzo P., Milano G., Musto P., Guerra G., *Macromolecules* **2003**, (36), 8695. (b) Albunia A.R,. Milano G, Venditto V., Guerra G., *Journal of the American Chemical Society,* **2005**, (127), 13114. (c) Venditto V.,. De Girolamo DM A,

Mensitieri G., Milano G., Musto P., Rizzo P., Guerra G., *Chemistry of. Materials*. **2006**, (18), 2205.

17. a) Annunziata L., Albunia A. R., Venditto V., Mensitieri G., Guerra G., *Macromolecules,* **2006**, (39), 9166; b) Guerra G., Manfredi C., Musto P., Tavone S., *Macromolecules,* **1998**, (31), 1329; c) Musto P., Manzari M., Guerra G., *Macromolecules,* **1999**, (32), 2770; d) Musto P., Rizzo P., Guerra G., *Macromolecules,* **2005,** (38)*,* 6079.

18. a) Di Molfetta A., Sethi R., *Environment Geology,* **2006**, (50), 361; b) Jeen S.-W., Jambor J. L., Blowees D. W., Gillham R. W., *Environmental Science of Technology,* **2007**, (41), 1989

19. Stanzel M. H., *Chem. Eng. Prog.,***1993**; (89), 36.

Chapter 3

Chiral co-crystalline phases PPO/alpha pinene

3.1 Introduction

As already shown in Chapter II, the PPO gels obtained in tetralin, decalin and α-pinene present the same type of crystalline structure which have been attributed to a co-crystalline phase on the basis of previous works reported in the literature.[1]

During this research project, the PPO/α-pinene co-crystalline structure has been deeply studied and in particular, the preparation procedures, the thermal stability of the co-crystalline phase as well as the conditions suitable for α-pinene removal (leading to a nanoporous crystalline phase) or for α-pinene sorption in the nanoporous crystalline phase (leading to the co-crystalline phase) have been investigated. An accurate structural analysis of the powder diffraction patterns has been carried out by Prof. V. Petraccone and Dr. O. Tarallo from the Dipartimento di Chimica "Paolo Corradini" of the Università degli Studi di Napoli Federico II and it has been established the occurrence of a chiral unit-cell including all right or left handed polymer helices and (1S)-(−) or (1R)-(+) α-pinene guest molecules, respectively. The formation of a chiral PPO/α-pinene co-crystalline form has been confirmed by vibrational circular dichroism (VCD) experiments.

3.1.1 Preparation, thermal behavior and molar ratio of the PPO/α-pinene co-crystalline form

As well described in the literature, the PPO/α-pinene co-crystalline phase can be easily obtained both by solution casting procedures and α-pinene induced crystallization in amorphous samples at high temperatures.[1-2]

An alternative route to prepare the PPO/α-pinene co-crystalline phase involves gel preparation but during air desorption of α-pinene there is a progressive loss of crystallinity which ends to a fully amorphous sample for a totally desiccated gels. However, when α-pinene is removed with supercritical CO_2, a crystalline nanoporous structure is obtained.

These results reported in Chapter II are summarized in Figure 3.1 which shows the X-ray diffraction patterns of the native PPO/α-pinene gel prepared at C_{pol}, = 20 wt% (curve A), and partially desiccated gels obtained by solvent desorption in air (curves B-D).
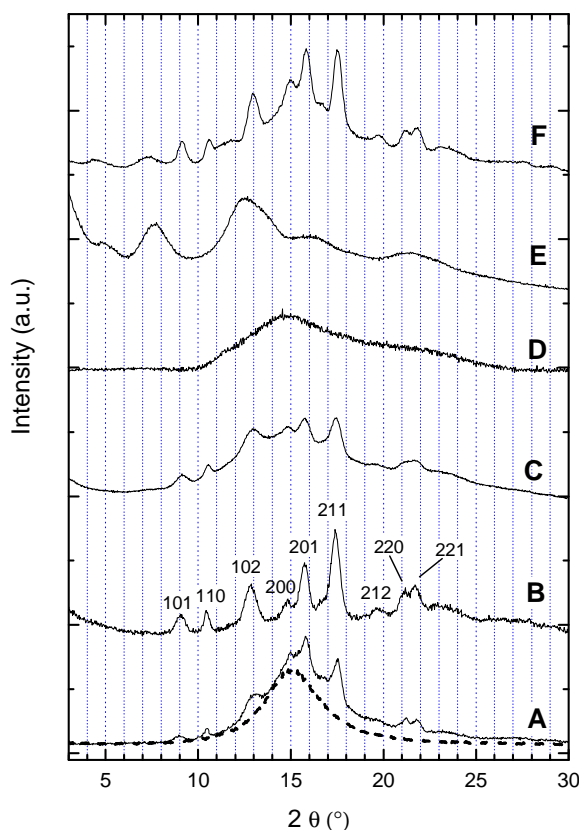
Figure 3.1 *X-ray diffraction patterns (CuKα radiation) of PPO samples: (A) gel with 80wt% of α-pinene and exhibiting the co-crystalline phase, the dashed line corresponds to the diffraction of liquid α-pinene; (B) powder with 33 wt% of α-pinene and exhibiting the co-crystalline phase, as obtained from the gel after long term solvent desorption at room temperature; (C) powder with 12 wt% of α-pinene as obtained from the co-crystalline powder after treatment at 80°C for two weeks; (D) amorphous powder with 7 wt% of α-pinene, as obtained from the co-crystalline powder after treatment at 140°C for 15 min; (E) powder exhibiting a nanoporous crystalline form, as obtained by complete α-pinene extraction with supercritical carbon dioxide from the gel of Figure A; (F) powder with 38 wt% of α-pinene and exhibiting the co-crystalline phase, as obtained from the nanoporous crystalline powder of Figure E after exposure for 1 hour to α-pinene vapor at 140°C. The Miller indexes of the PPO/α-pinene co-crystalline phase are indicated close to the plot B.*

The diffraction pattern of the native gel (curve A) already exhibits well defined diffraction peaks corresponding to the 101, 110, 102, 200, 201, 211, 220 and 221 reflections of the PPO/α-pinene co-crystalline form.[2b] These peaks are superimposed on an intense amorphous halo, which essentially corresponds to that one of liquid α-pinene (dashed line in Figure 3.1A).

The gel of Figure 1A, after long term (50 days) solvent desorption at room temperature becomes a powder with a α-pinene content close to 33 wt% and presents the X-ray diffraction pattern shown in Figure 1B, which is typical of the PPO/α-pinene co-crystalline phase.[2b] The degree of crystallinity, as evaluated by applying the standard procedure of resolving the diffraction pattern into two areas corresponding to the contributions of the crystalline and amorphous fractions, is

close to 67%. In the hypothesis that most α-pinene molecules are included in the PPO/α-pinene co-crystalline phase, this co-crystalline phase would be characterized by a monomeric-units/guest molar ratio close to 1.5. However, the subtraction of the amorphous halo of α-pinene from the pattern of Figure 1B indicates that roughly 20% of the guest is located in the amorphous polymer phase ($x_{am(\alpha\text{-pinene})} = 0.2$) and, as a consequence, the PPO/α-pinene co-crystalline phase exhibits a monomeric-units/guest molar ratio close to 2.

The thermal stability of the co-crystalline structure has been studied by thermogravimetric and X-ray diffraction measurements. The TGA curve of Figure 3.2A clearly shows that the guest loss begins above 70°C and diffraction results show a loss of crystallinity when guest desorption occurs. Just as an example, the X-ray diffraction pattern of the sample of Figure 3.1B, after treatment at 80°C for two weeks, shown in Figure 3.1C, still presents a pinene content close to 12 wt % and the typical peaks of the co-crystalline phase superimposed on an increased amorphous halo, corresponding to a reduced degree of crystallinity close to 30%.

Thermal treatments of the co-crystalline samples at higher temperatures lead to complete loss of crystallinity. This is shown, for instance, for a co-crystalline sample, which after treatment at 140°C for 15 min maintains a residual α-pinene content close to 7 wt% (as shown by the TGA curve of Figure 2B) and presents an X-ray diffraction with the typical diffraction amorphous halo of PPO (Figure 3.1D).

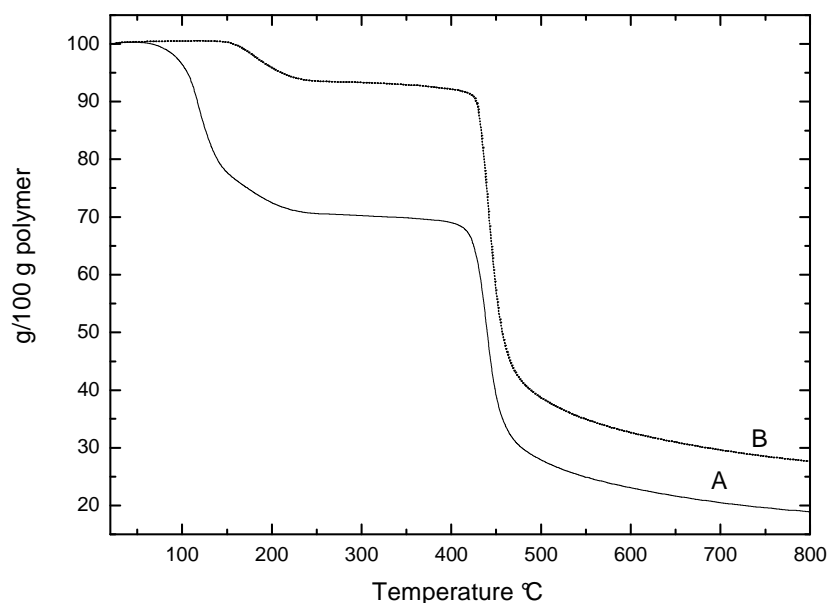***Figure 3.2.*** *Thermogravimetric curves of PPO powders: (A) exhibiting the PPO/α-pinene co-crystalline phase, as obtained from the gel after long term solvent desorption at room temperature, whose X-ray diffraction pattern is shown in Figure 3.1B; (B) amorphous powder, as obtained from the co-crystalline powder after treatment at 140°C for 15 min, whose X-ray diffraction pattern is shown in Figure 3.1D.*

By extraction with supercritical carbon dioxide at 40°C, the guest can be removed both from the amorphous and the co-crystalline phases of the PPO gel and a nanoporous crystalline phase is obtained. For instance, the X-ray diffraction pattern of the gel of figure 3.1A, after treatment with supercritical CO_2, is shown in figure 3.1E and presents diffraction peaks very similar to those of the nanoporous crystalline phase obtained by solvent extraction from carbon tetrachloride gels.[3] The degree of crystallinity of the nanoporous crystalline sample of figure 3.1E is about 48wt %.

The same procedure of α-pinene removal from the co-crystalline phase of powder samples (like that one of figure 3.1B) rather than from a gel sample (like that one of figure 3.1A) leads to fully amorphous samples. This suggests that the PPO/α-pinene co-crystalline phase can be reorganized in a nanoporous crystalline phase only in the presence of the more mobile gel environment.

This behavior is different from that one observed for s-PS, whose nanoporous δ phase can be obtained by guest extraction with supercritical carbon dioxide both from gel samples[4] as well from co-crystalline samples.[5]

This nanoporous crystalline phase, as well as the other nanoporous crystalline phases of PPO,[3] can be transformed into the co-crystalline phase by exposure to α-pinene vapor, at high temperatures. Just as an example, the nanoporous crystalline powder of figure 3.1E, after exposure for 1 hour to α-pinene vapor at 140°C, shows the X-ray diffraction pattern of figure 3.1F, which clearly indicates the presence of a well formed co-crystalline phase.

3.2 Structure of the PPO/α-pinene co-crystalline form

3.2.1 Unit cell

Unoriented co-crystalline samples of poly(2,6-dimethyl-1,4-phenylene)oxide (PPO) containing both racemic α-pinene, (1*R*)-(+)-α-pinene and (1*S*)-(−)-α-pinene have been prepared from the corresponding gels by partial solvent desorption in air.

The X-ray diffraction patterns of the powders are shown in Figure 3.3 (curve A-C) along with the X-ray diffraction pattern of reported in ref.2b.
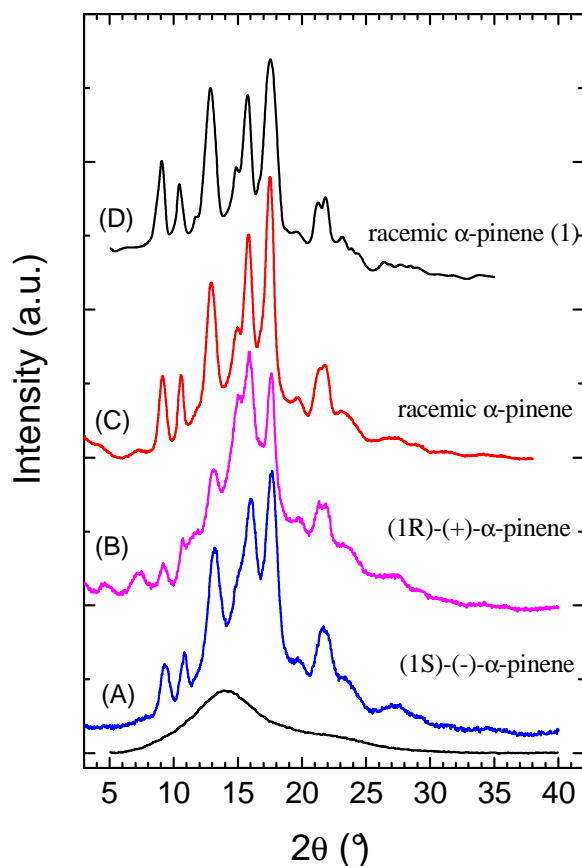
Figure 3.3 *X-ray diffraction patterns of PPO co-crystalline samples containing: (A) racemic α-pinene, (B) (1S)-($-$)-α-pinene and (C) (1R)-(+)-α-pinene. In (D) the X-ray diffraction pattern reported in ref.9c is reported for comparison.*

The powder X-ray diffraction patterns turned out to be very similar to each other and to that presented in literature by ref.9c both for positions and for relative intensities of the reflections (see Figure 3.1 and Table 3.1).

In the same paper,[2b] on the basis of both an unoriented X-ray diffraction pattern (shown in Figure 3.1E) and of an electron diffraction pattern collected on a single crystal, a tetragonal unit cell with $a=b=$ 1.19 nm and $c=$ 1.71 nm containing 4_1 helices has been proposed too.

It is worth pointing out that by arranging in the proposed unit cell two 4_1 polymer chains and four guest molecules the calculated density is 1.03 g/cm^3, in good agreement with the experimental one, determined by flotation ($\cong$ 1 g/cm^3).

Consequently, the unit cell proposed in ref.2b has been adopted for the structural analysis.

Table 3.1. *Diffraction angles (2θ °), Bragg distances (d_{obsd}) and relative intensities (after subtraction of the amorphous and background contribution, I_{obsd}) of the reflections observed in the X-ray powder diffraction patterns of Figures 3A,B and D. The patterns correspond to co-crystalline phases of PPO with racemic or non-racemic α-pinene molecules.*
The hkl indices, attributed according the tetragonal unit cell (a=1.19 nm, c= 1.71nm) proposed in ref.9c have been also reported.

	hkl	Ref.2b, Figure 3.3D, racemic guest		Figure 3.3B, non-racemic guest		Figure 3.3A, racemic guest	
		$2\theta_{obsd}$ (deg)	d_{obsd} (nm)	$2\theta_{obsd}$ (deg)	d_{obsd} (nm)	$2\theta_{obsd}$ (deg)	d_{obsd} (nm)
						7.25	1.020
1	101	9.0	0.983	9.3	0.947	9.14	0.968
2	110	10.4	0.851	10.9	0.813	10.6	0.839
3	111	11.8	0.750				
4	102	12.8	0.692	13.3	0.668	12.9	0.685
5	200	14.8	0.599			14.9	0.593
6	201	15.8	0.562	16.2	0.549	15.8	0.560
7	210	16.7	0.531				
8	211	17.4	0.510	17.8	0.499	17.5	0.507
9	212	19.6	0.453	19.8	0.448	19.7	0.451
10	220	21.2	0.420			21.4	0.416
11	221	21.7	0.410	21.8	0.408	21.8	0.310
12	301	23.0	0.387	23.5	0.379	23.1	0.385
13						26.7	0.334
				27.4	0.325	27.4	0.325
						29.1	0.307
				31.5	0.284		

3.2.2 Polymer Conformation

The chain conformation has been found from molecular mechanics calculations by imposing P4$_1$ (P4$_3$) symmetry and the *c* periodicity (1.71 nm) suggested in ref.2b and found also in the case of PPO crystallized from chloroform solutions.[6] A schematic representation of the conformation that has been used as the starting point for the subsequent structural analysis is reported in Figure 3.4. The most relevant internal parameters are also shown.
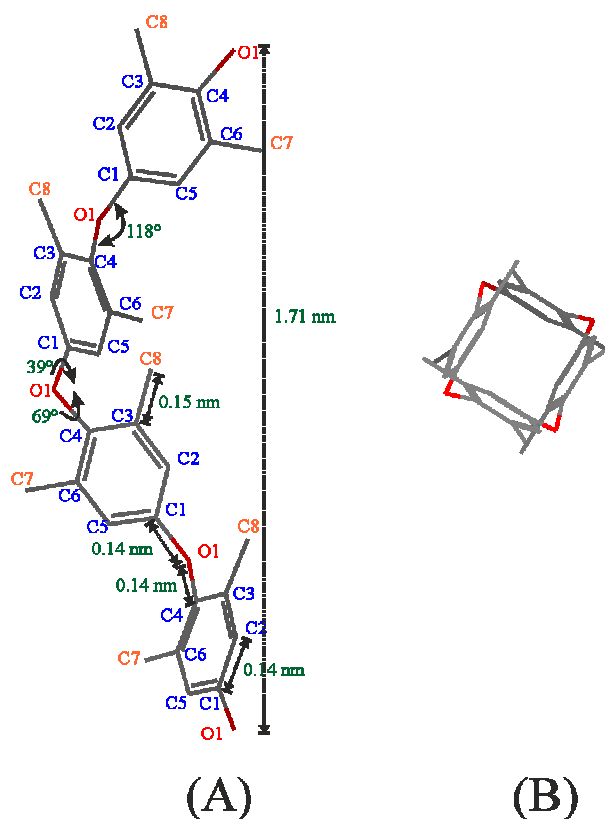
Figure 3.4 *Conformation of the PPO chain as found by molecular mechanics calculations*

3.2.3 Space group

For packing analyses, on the basis of the content of the unit cell and in the likely hypothesis that the 4_1 symmetry of the polymer chain would be kept, the space group $P4_1$ ($P4_3$) with two independent polymer helices has been chosen . The asymmetric unit is made of a repeating unit of a polymer chain plus another one belonging to a second independent polymer chain, and a guest molecule.

Due to the likeness of all the powder diffraction patterns of Figure 3.3, in the search for the packing model a model with ($1S$)-($-$)-α -pinene as guest and R polymer helices (space group $P4_1$) or L polymer helices (space group $P4_3$) has been first used. In each case the possibility to have an isoclinic or anticlinic packing of the independent helices has been also considered.

3.2.4 Packing model

In these hypotheses, through molecular mechanics calculations, a structural model characterized by good packing has been searched. In particular several starting points have been explored, starting from different situations (found by a trial and error procedure) characterized by different rotations of the polymer helices around the chain axis, different relative quota along the *c* axis direction, and different arrangement of the pinene guest molecule. For each one of the minimum energy model

52

obtained a careful comparison between the experimental and the calculated powder X-ray diffraction pattern was carried out.

The best packing model obtained, both as far as the lowest packing energy and for the agreement with the calculated diffraction pattern with the experimental one, is reported in figure 3.5 (its fractional coordinates for the asymmetric unit are listed in Table 3.2).
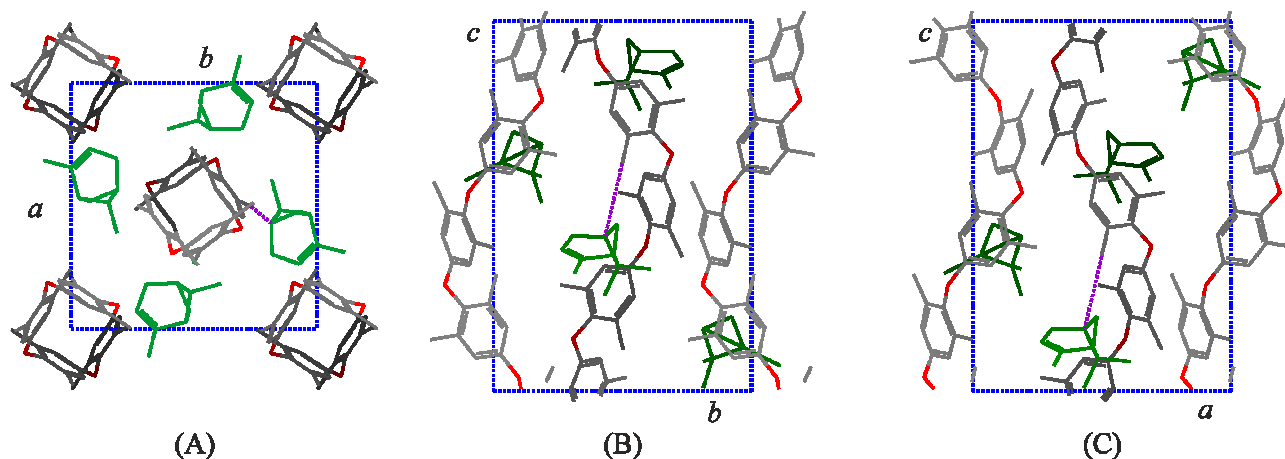
Figure 3.5 *Packing model of the co-crystalline form of PPO with (1S)-(−)-α-pinene in the unit cell a=b=1.19 nm and c=1.71 nm , and the P4₃ space group. (A) Projection along c; (B) projection along a; (C) projection along b.*

Figure 3.5 shows the comparison between the calculated X-ray powder diffraction profile according the structural model of Figure 3.4 vs. the experimental X-ray powder diffraction pattern (reported in Figure 3.2), after subtraction of the amorphous and background contributions. A fairly good agreement is apparent.

Figure 3.6 *Comparison between the experimental X-ray powder diffraction pattern (black solid line) of the co-crystalline form of PPO with (1S)-(−)-α-pinene after subtraction of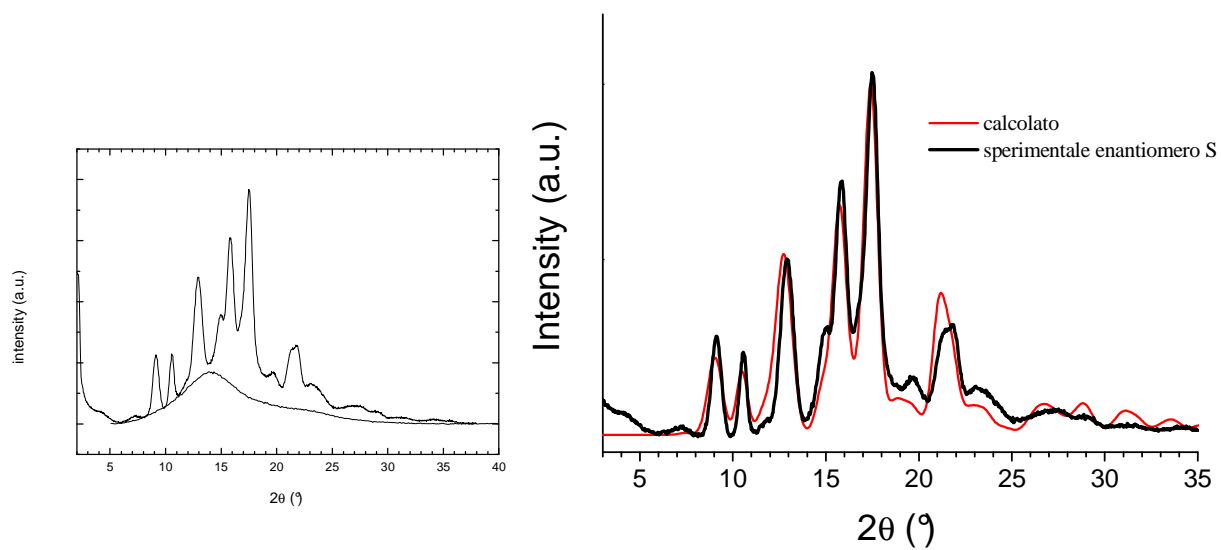 the amorphous and background halos (figure 3.2) with the calculated one (red solid line) according to the structural model proposed in figure 3.4.*

Table 3.2 *Fractional coordinates of the atoms of the asymmetric unit of the co-crystalline form of PPO with (1S)-(−)-α-pinene according the model reported in Figure 5 (cell constants a = b = 1.19 nm, c = 1.71 nm; space group P4₃). The fractional coordinates of the atoms of the guest are reported in italics. Hydrogen atoms were included in the structure factors calculation, but they are omitted in this table for simplicity.*

	x/a	y/b	z/c
C1	0,159	0,028	0,098
C2	0,199	0,052	0,173
C3	0,179	-0,018	0,236
C4	0,114	-0,114	0,226
C5	0,071	-0,139	0,152
C6	0,094	-0,069	0,089
O1	0,098	-0,190	0,286
C7	0,231	0,010	0,315
C8	0,002	-0,243	0,138
C1b	-0,477	0,658	0,579
C2b	-0,455	0,701	0,505
C3b	-0,523	0,679	0,441
C4b	-0,617	0,609	0,451
C5b	-0,638	0,562	0,525
C6b	-0,570	0,587	0,587
O1	-0,692	0,591	0,391
C7b	-0,498	0,731	0,363
C8b	-0,739	0,487	0,537
C	*0,001*	*0,342*	*0,357*
C	*-0,073*	*0,266*	*0,382*
C	*-0,184*	*0,305*	*0,418*
C	*-0,187*	*0,432*	*0,417*
C	*-0,076*	*0,479*	*0,451*
C	*-0,030*	*0,467*	*0,367*
C	*0,112*	*0,314*	*0,319*
C	*-0,150*	*0,484*	*0,338*
C	*-0,186*	*0,431*	*0,259*

A more detailed representation of the accommodation of the guest in the space delimited by the polymer helices according the model of Figure 3.5, highlighting also the shape of the guest locations in the co-crystalline form, is reported in Figure 3.7.
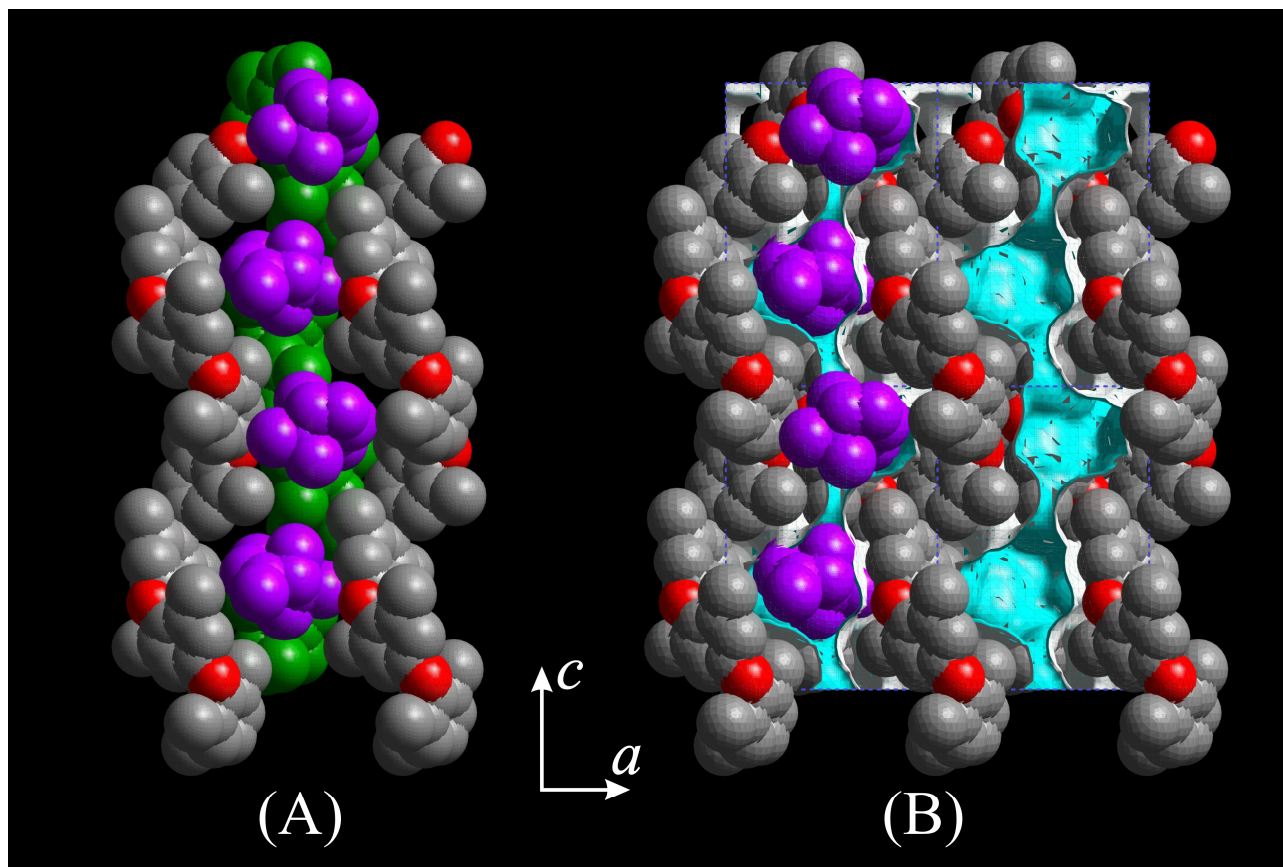
Figure 3.7 *Schematic representation the minimum energy arrangements of the (1S)-(−)-α-pinene guest molecules in the guest locations of the PPO co-crystals found by molecular mechanics calculations. (a, a') view of a cavity along the a axis. (b, b') view of a cavity along the b axis. In (a') and (b') guest molecules are represented with their van der Waals steric hindrance. The chain repetition period is indicated by dashed lines. The shape of the space where the guest molecules are hosted is also represented. The internal face of the space occupied by the α-pinene molecules is reported in cyan while the external face (towards the chains) is reported in white. In B only the portion of the channels passing through eight neighboring cells are shown, while the polymer helices are omitted. R = right handed, L = left handed helical chains.*

As expected, the same results have been obtained for the clathrate structure of PPO with (1*R*)-(+)-α-pinene according the P4$_1$ space group.

The possibility to have also non chiral crystals, i.e. packing models characterized by an analogous arrangements of the polymer helices according to the P4$_3$ and P4$_1$ space groups but hosting (1*R*)-(+)-α-pinene or (1*S*)-(−)-α-pinene, respectively has been also widely explored. Despite several promising models characterized by energetically favorable packing have been found, the agreement between the experimental and the calculated diffraction pattern was always poor.

It is worth noting that, co-crystalline phases of PPO with racemic α-pinene guest molecules, because present X-ray powder diffraction patterns essentially indistinguishable from those of co-crystalline phases with the pure enantiomers (figure 3.3), are expected to be constituted by a

mixture. of chiral crystals including only L and R polymer helices and S and R α-pinene enantiomers, respectively.

3.3 VCD and FTIR measurements

In order to confirm the formation of a chiral PPO/α-pinene co-crystalline phases vibrational circular dichroism experiments have been carried.

3.3.1 Introduction

The interaction between light and a chiral molecule depends on the circular polarization of the probing light. The adsorbance A of right-circularly- R polarized light by a "right-handed" will be equal to the absorbance A of left-circularly L polarized light by the corresponding of "left-handed" enantiomer. If the light is polarized probing a symmetric molecule lacking directions. a chiral center or a racemic mixture (equal mixture of the enantiomers), then clearly $A_L - A_R = 0$. But so long as there is an excess of one form or the other of a given chiral species, the differential absorption of left- versus right-circularly polarized light $A_L - A_R$ will not be zero, as shown in figure 3.7.

left circularly
polarized light   chiral molecule A_L

right circularly
polarized light   chiral molecule A_R

$$A_L - A_R = \Delta A$$
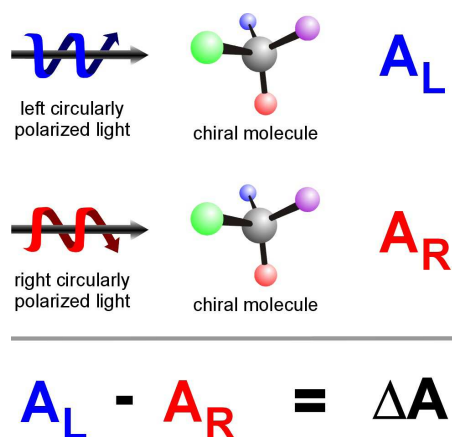
The quantity $\Delta A = A_L - A_R$ depends on the wavelength and is termed the circular dichroism; it represents a measure of the chirality of the probed species and determines the direction and degree of rotation of the lane of linearly polarized light. Note that the sign and magnitude of ΔA is determined by the specific orientation and polarizability of the atoms or groups around a chiral center; ΔA can be either positive or negative for a given configuration (e.g. *(R)*- applications have been enantiomer) but will always be equal in magnitude and opposite in sign for *R* vs. *S* enantiomers.

The chirality of a molecule not only determines certain physical properties such as crystal structure and dichroism more importantly, also its chemical reactivity. Two molecules must have the appropriate handedness stereochimistry in order to combine or react. This stereospecificity of

reaction mechanisms is of crucial importance in biochemistry where most enzymic reactions require a specific configuration or conformation of the reacting species.

The measurement of Circular Dichroism (CD) as a function of wavelength in the visible and UV region has been possible with a commercial instrumentation for some time, but applications have been limited.

In CD the absorption bands are usually rather broad, and measurements are often limited by the low sample concentrations required (particularly for biomolecules) due to high extinction coefficients and scattering effects (the latter are particularly troublesome in the UV/vis range).

If CD measurements are carried out in the infrared region, the method is termed vibrational circular dichroism or VCD, which is defined as the difference in absorption of a sample for left vs. right circularly polarized infrared radiation $\Delta A = A_L - A_R$. VCD has some very distinct advantages: most molecules have significant IR absorption cross sections; sharp IR lines are associated with specific vibrational modes and more structural information can be obtained from a VCD measurement than from a CD spectrum. The advantage of the VCD spectroscopy is that two enantiomers exhibit VCD spectra with the same features but with opposit sign. An equivalent mixture of two enantiomers, a racemic mixture, shows no VCD signal intensities. This behaviour leads to the possibility of the determination of the optical purity, the enantiomeric excess, after appropriate calibration of the investigated system. Another application arises from the fact that the two enantiomers have VCD spectra with opposite sign, they are clearly distinguishable.

3.3.2 Experimental results

Co-crystalline powders with a α-pinene content close to 30wt%, exhibiting co-crystalline phases with (1*R*)-(+)-α-pinene or (1*S*)-(−)-α-pinene enantiomers (whose X-ray diffraction patterns are similar to those of Figure 3.2) have been prepared by guest sorption at 140°C in nanoporous crystalline powders, like that one of Figure 3.1E, as crystallized in the presence of an achiral solvent.

The IR and VCD spectra of PPO powder samples exhibiting co-crystalline phases with α-pinene enantiomers are shown, for the wavenumber range 1650-1050 cm^{-1}, in figures 3.8A and 3.8B, respectively.

The IR spectrum shows beside intense PPO peaks also α-pinene peaks at 1365 cm^{-1} (vibrational mode 45), 1265 cm^{-1} (vibrational mode 41), 1215 cm^{-1} (shoulder, vibrational mode 38) e 1125 cm^{-1} (vibrational mode 34). [7]

The VCD spectrum shows beside two α-pinene peaks at 1215 and 1125 cm^{-1} (i.e. the α-pinene most dichroic peaks),[7] more intense PPO peaks. In particular, the intense absorption band centered at 1187 cm^{-1} give rise to two intense VCD peaks of opposite sign centered at 1197 and 1174 cm^{-1}. Analogously, the PPO absorption band centered at 1306 cm^{-1} give rise to two VCD peaks of opposite sign centered at 1310 and 1300 cm^{-1}.

The results of figure 3.8 indicate that PPO chains become chiral as a consequence of co-crystallization with non-racemic α-pinene molecules. This result is, of course, easily rationalized by the chiral structures including only L or R polymer helices and S or R α-pinene enantiomers, respectively, as proposed by the X-ray diffraction study of the previous section.

It is worth adding that, for PPO co-crystalline phases with non-racemic α-pinene guest molecules, the VCD behavior described in Figure 3.8 is observed independently of the preparation procedure. For instance, VCD spectra strictly similar to those reported in figure 3.8B are observed for co-crystalline samples (films or powders) as obtained by α-pinene induced crystallization in amorphous PPO films (sorption at 140°C).
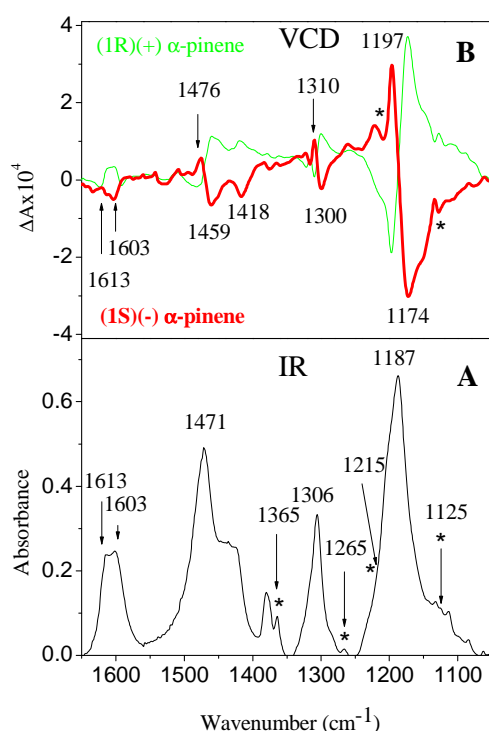
Figure 3.8 FTIR (A) and VCD spectra (B) of PPO powders, exhibiting co-crystalline phases with (1R)-(+)-α-pinene (thin green line) or (1S)-(−)-α-pinene (thick red line) and an α-pinene content close to 30 wt%. The α-pinene peaks are indicated by a star (*)

Gels exhibiting PPO co-crystalline phases with a (1R)-(+)-α-pinene or (1S)-(−)-α-pinene enantiomers, whose X-ray diffraction patterns are similar to that one of Figure 1A, when fully

extracted by supercritical carbon dioxide are transformed in nanoporous-crystalline powders, whose X-ray diffraction patterns are strictly similar to that one of Figure 1E. The obtained nanoporous-crystalline samples, although co-crystallized in the presence of non-racemic α-pinene, do not present any VCD peak.

In summary, for PPO, co-crystalline phases with non-racemic guest molecules, present intense VCD phenomena, independently of their preparation procedure while nanoporous-crystalline phase do not present VCD phenomena, also when prepared from non-racemic co-crystalline phases.

This behaviour is completely different from that one observed for s-PS, whose co-crystalline phases with non-racemic guest molecules, present intense VCD phenomena, only if induced by non-racemic guests in amorphous samples[8] (and never starting from crystalline s-PS samples)[8b-d] while intense VCD phenomena are observed for all other crystalline phases, if prepared from non-racemic co-crystalline phases.

These completely different behaviors can be easily rationalized by the fact that the CD phenomena observed for s-PS are due to chiral morphologies[8] of the crystallites while for PPO/α-pinene co-crystalline samples are due to the chirality of the crystalline unit cell.

3.3.3 Comments on the Structure of the nanoporous Crystalline Phases

The absence of fiber samples and literature data about the PPO nanoporous phases (i.e. unit cell parameters and chain conformation) did not allow us to carry out a detailed structural analysis of the PPO crystalline phases.

However, some preliminary FTIR studies were performed to possibly gain information on the conformation of the chains in the nanoporous phases.

In Figure 3,9 are reported the IR spectra in the 910-400 cm^{-1} wavenumber range of amorphous and semi-crystalline PPO films characterized by the α-pinene co-crystalline phase and by two nanoporous crystalline phases.
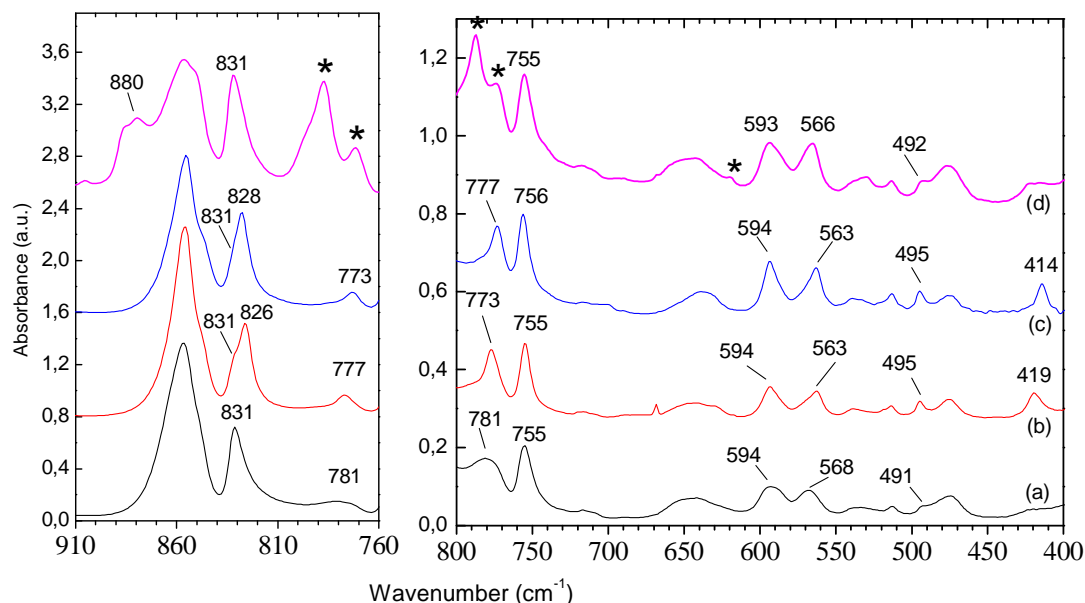
Figure 3.9 *IR spectra of a PPO amorphous film sample (curve a), semi-crystalline film samples obtained by sorption of benzene (b) or CCl₄ (c) in amorphous PPO followed by complete solvent extraction by supercritical carbon dioxide and clathrate PPO/α-pinene film. The 910-400 cm⁻¹ wavenumber region has been split in two graphs for the sake of clarity.*
The (*) indicate the α-pinene peaks.

We can observe in Figure 3,9 that the IR spectrum of a fully amorphous PPO sample (curve a) in the 910-400 cm⁻¹ region is markedly different from those of semi-crystalline PPO samples. In particular: i) the broad bands of amorphous PPO located at 781, 594, 563 and 491 becomes sharper in semi-crystalline samples; ii) in the 410-420 cm⁻¹ region, the semi-crystalline samples display a sharp IR band which is absent in the amorphous PPO. iii) the IR spectrum of amorphous PPO presents a sharp band at 831 cm⁻¹ which becomes, in semi-crystalline PPO samples, the shoulder of a new band located at a lower wavenumber.

It is also worth noting that the IR spectra of semi-crystalline PPO are overall similar but significant variations due to the different the chain packing in the nanoporous crystalline phase can be observed. In particular the crystalline sample crystallized with benzene (curve b) presents sharp band located at 826, 777, and 419 cm⁻¹ while the CCl₄ crystallized PPO (curve c) presents bands located at 828, 773, and 414 cm⁻¹.

Finally, the IR spectrum of the clathrate sample PPO/α-pinene presents at 880 cm⁻¹ a sharp band that not appear in the amorphous and semicrystalline sample.

These results show that the amorphous sample, the crystalline and the clathrate PPO/α-pinene present different conformation of the chains.

CONCLUDING REMARKS

Preparation procedures, thermal properties, polymorphic behavior and crystal structure of co-crystalline phase of PPO with α-pinene have been deeply characterized. New preparation procedures, based on gel formation or on high-temperature α-pinene sorption in PPO nanoporous crystalline phases, have been described. The co-crystalline phase presents a long-term stability up to 70-80°C while progressively becomes fully amorphous for thermal treatments at higher temperatures. It becomes amorphous also as a consequence of α-pinene extraction by supercritical carbon dioxide.

However, the same procedure of α-pinene extraction, when applied to gel samples exhibiting the PPO/α-pinene co-crystalline form, leads to powders exhibiting X-ray diffraction patterns typical of the nanoporous-crystalline modification obtained from CCl_4 gels. The crystalline phase obtained from α-pinene gels presents high sorption ability, toward many organic compounds, as recently described for other PPO nanoporous-crystalline phases. For instance, the α-pinene uptake from 2 ppm aqueous solutions is as high as 8.5 wt%.

X-ray diffraction data on unoriented PPO samples exhibiting co-crystalline phases with racemic and non-racemic α-pinene guest molecules and the related X-ray diffraction analyses have allowed a complete resolution of the co-crystalline structure.

The described PPO/α-pinene co-crystalline structure, presenting the tetragonal unit cell ($a=1.19$ nm, $c=1.71$nm) already proposed in ref.9c, is characterized by a monomer-unit/guest ratio equal to 2:1 and has been found to be chiral, i.e. the unit cell includes all right or left handed polymer helices and (1S)-(−) or (1R)-(+) α-pinene guest molecules, respectively.

The chirality of the co-crystalline structure has been clearly confirmed by vibrational circular dichroism (VCD) measurements for samples including PPO co-crystalline phases with non-racemic α-pinene molecules. In fact, intense VCD peaks are observed for PPO, which are also more intense than those observed for the non-racemic guest.

It is worth adding that this is the first crystalline structure reported for PPO that is an industrially relevant specialty polymer.

REFERENCES

1. Hurek J., Turska E., *Acta Polimerica,* **1984**, (35)*,* 201.

2. a) Barrales-Rienda M., Fatou J.M.G., *Kolloid-Z.u.Z.Polym.* **1971**, (244), 317; b) Horikiri, S. *Journal of Polymer Science-A2,* **1972**, (10)*,* 1167.

3. Daniel C., Longo S., Fasano G., Vitillo J.G., Guerra G., *Chemistry of Materials,* **2011**, (23), 3195.

4. a) Daniel C., Alfano D., Venditto V., Cardea S., Reverchon E., Larobina D., Mensitieri G., Guerra, G., *Advanced Materials,* **2005**,(17)*,*1515; b) Daniel C., Sannino D., Guerra G., *Chemistry of Materials,* **2008**, (20), 577.

5. a) Reverchon E., Guerra G., Venditto V., *Journal of Applied Polymer Science* **1999**, (74), 2077; b) Ma W., Yu J., He J., *Macromolecules* **2005**, (38), 4755.

6. Factor A., Heinsohn G. E., Vogt L. H., Jr.. *Journal of Polymer Science, Polym.Lett.Ed.* **1969**, (7), 205.

7. Devlin F.J., Stephens P.J., Cheesemann J.R., Frisch M.J., *Journal of Physical Chemistry, A.* **1997**, (101), 9912.

8. a) Buono A., Immediata I., Rizzo P., Guerra G., *Journal of the American Chemical Society,* **2007**, (129), 10992; b) Guadagno L., Raimondo M., Silvestre C., Immediata I., Rizzo P., Guerra G., *Journal of Materials Chemistry,* **2008***,* (18), 567; c) Rizzo P., Beltrani M., Guerra G., *Chirality,* **2010**, (22), E67; d) Rizzo P., Montefusco T., Guerra G., *Journal of the American Chemical Society,* **2011**, (133), 9872.

Chapter 4

EXPERIMENTAL SECTION

4.1 Materials and Sample preparation

The isotactic poly(4-methyl-pentene-1) (P4MP1) and the poly(2,6-dimethyl-1,4-phenylene oxide) (PPO) polymers used in this study were purchased from Aldrich. All the solvents were purchased from Aldrich and used without further purification.

4.1.1 P4MP1

P4MP1 gel samples were prepared in hermetically sealed test tubes by heating the mixtures until complete dissolution of the polymer and the appearance of a transparent and homogeneous solution had occurred. For cyclopentane gels, polymer was dissolved at 85°C while with the other solvents polymer was dissolved at 160°C. Then the hot solution was cooled down to room temperature where gelation occurred.

Aerogel samples were obtained by treating native gels with a SFX 200 supercritical carbon dioxide extractor (ISCO Inc.) using the following conditions: T= 40°C, P = 200 bar, extraction time t = 240 min.

For monolithic aerogels with a regular shape (i.e sphere, or cylinders) the total porosity, including macroporosity, mesoporosity and micorporosity, can be estimated from the volume/mass ratio of the aerogel.

Then, the percentage of porosity P of the aerogel samples can be expressed as:[1]

$$P = 100\left(1 - \frac{\rho_{app}}{\rho_{pol}}\right)$$

where ρ_{pol} is the density of the polymer matrix (e.g., equal to 0.83 g/cm^3 and 1.06 g/cm^3 for semicrystalline P4MP samples with a crystallinity of 50%, exhibiting Form I and Form II phases, respectively) and ρ_{app} is the aerogel apparent density calculated from from the mass/volume ratio of the monolithic aerogels.

4.1.2 PPO

The PPO used in this study was purchased by Sigma Aldrich and presents weight-averaged and number-averaged molecular masses M_w= 244000 and M_n= 32000, respectively.

PPO gel samples were prepared in hermetically sealed test tubes by heating the mixtures above the boiling point of the solvent until complete dissolution of the polymer and the appearance of a transparent and homogeneous solution had occurred. Then the hot solution was cooled down to room temperature where gelation occurred.

PPO powders were obtained by treating these gels with a SFX 200 supercritical carbon dioxide extractor (ISCO Inc.) using the following conditions: T= 40°C, P = 250 bar, extraction time t = 300 min. PPO amorphous powders have been obtained by treating PPO/decalin gels with the same carbon dioxide extractor, for 16 hours.

PPO amorphous films, 50-100 μm thick, were obtained by compression molding after melting at 290°C. The crystallization of these amorphous films has been induced by vapor sorption procedures at different temperatures. The solvent was removed from the crystallized films by the above described extraction procedure with supercritical carbon dioxide.

The density of film samples was determined by flotation, at room temperature, in aqueous solutions of $CaCl_2$.

4.2 Techniques

4.2.1 X-ray diffraction analysis

X-ray diffraction patterns were obtained on a Bruker D8 Advance automatic diffractometer operating with a nickel-filtered CuKα radiation. The degree of crystallinity of powders and films was obtained from the X-ray diffraction data, by applying the standard procedure of resolving the diffraction pattern into two areas corresponding to the contributions of the crystalline and amorphous fractions (in particulary for PPO in the 2θ range 6°-35°).

Evaluation of the correlation length D of the crystalline domains (where an ordered disposition of the atoms is maintained) was effected using the Scherrer formula:

$$D = 0.9\lambda / (\beta \cos\theta)$$

where β is the full width at half-maximum expressed in radian units, λ is the wavelength and 2θ the diffraction angle. The value of β was corrected from the experimental effects applying the procedure described in ref. 2.

4.2.2 X-ray diffraction analysis for co-crystalline PPO/α-pinene form

Wide-angle X-ray diffraction patterns of unoriented samples were obtained with nickel-filtered CuKα radiation with an automatic Philips powder diffractometer operating in the θ/2θ Bragg-Brentano geometry using specimen holders 2 mm thick.

Calculated X-ray powder diffraction pattern were obtained with the Diffraction-Crystal module of the software package Cerius[2] (version 4.2 by Accelrys Inc.) using an isotropic thermal factor (B = 8 Å^2). A Gaussian profile function having a half-height width regulated by the average crystallite size along *a*, *b*, and *c* axes (L_a, L_b and L_c, respectively) was used. A good agreement with the half-height width of the peaks in the experimental profile has been obtained for $L_a = L_b = 10$ nm and $L_c = 8$ nm.

As for co-crystalline samples (like those of Figures 3.1B,C), the degree of crystallinity has been evaluated as the difference between the weight percent of polymer in the sample (based on TGA measurements like those of Figure 3.2) and the weight percent of polymer amorphous phase in the sample (based on the amorphous areas of the X-ray diffraction patterns). The amount of α-pinene in the amorphous polymer phase, expressed as wt% of the overall sample, has been evaluated by the area of the amorphous pattern of the solvent (A[α-pinene, amorphous]) that can be subtracted from the pattern of the co-crystalline polymer sample (after subtraction of the polymer amorphous halo):

$$wt\%[\alpha\text{-pinene, amorphous}] = A[\alpha\text{-pinene, amorphous}]/ A_{tot}$$

Correspondingly, the guest fraction located in the amorphous phase, rather than in the co-crystalline phase, has been evaluated as:

$$x_{am}(\alpha\text{-pinene}) = \frac{wt\%[\alpha\text{-pinene, amorphous}]}{wt\%[\alpha\text{-pinene, sample}]}$$

where   wt%[α-pinene, sample] is evaluated by gravimetric measurements.

Energy calculation methods and shape of cavities.

Energy calculations were carried out by using the Compass[3] force field within the Open Force Field module of Cerius[2] by the smart minimizer method with standard convergence.

The shape of the cavities has been determined with the Free Volume module of Cerius[2] by calculating the region of the structure accessible to a probe species (with a radius of 0.1 nm) diffusing into the model from the exterior.

4.2.3 Fourier Transform Infrared and VCD measurements

Fourier Transform Infrared (FTIR) spectra were obtained at a resolution of 2.0 cm^{-1} with a Vertex 70 Bruker spectrometer equipped with deuterated triglycine sulfate (DTGS) detector and a

Ge/KBr beam splitter. The frequency scale was internally calibrated to $0.01 \ cm^{-1}$ using a He-Ne laser. 32 scans were signal averaged to reduce the noise.

VCD measurements were recorded using a commercial Bruker Tensor 27 FT-IR spectrometer coupled to a PMA50 external module, (needed to double modulate the Infrared radiation) using a linear KRS5 polarizer, a ZnSe 50 KHz photoelastic modulator (PEM, by HINDS) with a proper antireflecting coating, an optical filter (transmitting below $2000 \ cm^{-1}$) and a narrow band MCT (Mercury Cadmium Telluride) detector. All VCD spectra were recorded for 30 minutes of data collection time, at $4 \ cm^{-1}$ resolution. Samples were tested for satisfactory VCD characteristics by comparison of the VCD obtained with the film rotated by ±45°C around the light beam axis. However, to eliminate any possible linear dichroism influence, the VCD measurements have been conducted by averaging the spectra as collected for several different in-plane rotation angles.

4.2.4 Vapor sorption measurements

The vapor sorption measurements have been carried out at 35°C with a VTI-SA symmetrical vapor sorption analyzer from TA instruments. This instrument works in a continuous flow of gas and is designed to study the isothermal curves at temperatures ranging between 5-50 ° C at atmospheric pressure. The term "symmetrical" refers to the fact that the chambers of the microbalance, and that of the reference sample, are subject to the same conditions of temperature, relative humidity and flow rate. This allows a significant stability and accuracy.

4.2.5 TGA measurements

The content of the guest molecules in the films was determined by the intensity of FTIR guest peaks, as calibrated by thermogravimetric measurements. Thermogravimetric measurements (TGA) were performed with a TG 209 F1 equipment from Netzsch.

4.2.6 SEM Analysis

The internal morphology of the aerogelic monoliths was characterized by means of a scanning electron microscope (SEM, Zeiss Evo50 equipped with an Oxford energy dispersive X-ray detector). Samples were prepared by fracturing small pieces of the monoliths in order to make accessible the internal part of the specimen. In fact, the external lateral surface of all the samples resulted to be flat and free of porosity. Low energy was used (5 keV) in order to obtain the highest possible surface resolution. Before imaging, all the specimens were coated with gold using a VCR high resolution indirect ion-beam sputtering system. The samples were coated depositing

approximately 20 nm of gold. The coating procedure was necessary in order to prevent the surface charging during the measurement and to increase the images resolution.

4.2.7 Porosimetry

Surface area, pore volume and pore size distribution were obtained by N_2 adsorption measurements carried out at 77 K on a Micromeritics ASAP 2020 sorption analyzer.

Surface area, pore volume and pore size distribution were obtained by N_2 adsorption measurements carried out at 77 K on a Micromeritics ASAP 2020 sorption analyzer.

All the samples, were outgassed for 24 h at 30°C before the analysis.

In the case of the P4MP1/CP monolith a null surface area was obtained for the monolith as-prepared. In this case, the N_2 curves were obtained by fracturing the specimen in order to make accessible the internal pores of the material. The specific surface area of the polymers was calculated using the Brunauer–Emmet–Teller method,[3] while the pore diameter and the pore size distribution were evaluated using the DFT (Density Functional Theory) method on the basis of the cylindrical pore model proposed by Jaroniec et al.[4] The micropore volume has been determinate with the t-plot method,[5] adopting a new equation of thickness obtained using as master sample a bulk form a sPS delta phase (sPS thickness equation in the following). The thickness of the single molecular layer has been set to $\sigma = 3.54$ Å[6] and t has been obtained as $\dfrac{n}{n_m}\sigma$ (where n is the number of molecules adsorbed and n_m the value of n at the monolayer) according to the definition of t.[5]

References

1. Ko, E., *In Kirk-Othmer Encyclopedia of Chemical Technology*, 4th ed., John Wiley & Sons: New York, **1998**; Suppl. Vol., "Aerogel", pp 1-22.

2. Klug, H. P., Alexander L. E., In X-ray diffraction Procedures; John Wiley: New York, 1959; Chapter 9.

3. Brunauer, S.; Emmett, P. H.; Teller, E., *Adsorption of Gases in Multimolecular Layers*, **1938,** (60), 309.

4. Jaroniec, M.; Kruk, M.; Olivier, J. P.; Koch, S. In *A new method for the accurate pore size analysis of MCM-41 and other silica-based mesoporous meterials*, COPS-V, Heidelberg (D), **1999**.

5. Gregg, S. J.; Sing, K. S. W., Adsorption, Surface Area and Porosity. In Academic Press: London, **1982**; p 113.

6. Lippens, B. C., De Boer, J. H., Journal of Catalysis, **1965**, (4), 319.